Hydrous regions of the mantle transition zone lie beneath areas of intraplate volcanism

Helene Wang[1], Valentina Magni[2], Clinton P. Conrad[3], and Mathew Domeier[3]

[1]TGS
[2]Norwegian Geotechnical Institute (NGI)
[3]Universitetet i Oslo

September 27, 2024

Abstract

Great volumes of water are carried downward into the mantle transition zone (MTZ, 410-670 km depth) by subducting slabs. If this water is later drawn upward, the resulting mantle melting may generate intraplate volcanism (IPV). Despite its importance, the amount and spatial distribution of water within the MTZ, and its impact on IPV, are poorly constrained. Here we use a series of plate tectonic reconstructions to estimate rates and positions of water injection into the MTZ by subducted slabs during the past 400 Myr. This allows us to construct maps of heterogeneous MTZ hydration, which we then compare to IPV locations since 200 Ma. We find a statistically significant correlation between wet regions of the MTZ and locations of IPV at the surface, but only if water remains stored in the MTZ for periods of 30-100 Myr after being carried there by slabs. We find that 42-68% of IPV is underlain by wet MTZ, with higher correlations associated with longer MTZ residence time, slower slab sinking rates, and longer time periods between MTZ hydration and IPV eruption. The correlation is highest during the Jurassic, when more extensive slab interaction with the MTZ caused a wider area of the MTZ to become hydrated. Parts of the MTZ near the western Pacific, southern Africa, and western Europe, have remained dry by avoiding wet slabs. Hydrous upwellings rising from the MTZ, some driven by interactions with subducting slabs, may be responsible for IPV rising from wet MTZ regions.

Hydrous regions of the mantle transition zone lie beneath areas of intraplate volcanism

Helene Wang[1,2], Valentina Magni[1,3], Clinton P. Conrad[1,4,*] and Mathew Domeier[1,4]

[1] Centre for Earth Evolution and Dynamics (CEED), University of Oslo, Oslo, Norway
[2] TGS, Oslo, Norway
[3] Norwegian Geotechnical Institute (NGI), Oslo, Norway
[4] Centre for Planetary Habitability (PHAB), University of Oslo, Oslo, Norway
[*] Corresponding author: Clinton P. Conrad (c.p.conrad@geo.uio.no)

Manuscript submitted to *Geochemistry, Geophysics, Geosystems,* September 2024

Key Points:

- We use tectonic reconstructions of subduction history to map the hydration state of the mantle transition zone (MTZ) for the past 400 Myr.
- We identify a statistically significant correlation between hydrated MTZ and intraplate volcanism (IPV) at the Earth's surface.
- Hydrated MTZ can explain IPV if subducted water stalls in the MTZ for ~100 Myr and hydrous upwelling induces sub-lithospheric melting.

Abstract

Great volumes of water are carried downward into the mantle transition zone (MTZ, 410-670 km depth) by subducting slabs. If this water is later drawn upward, the resulting mantle melting may generate intraplate volcanism (IPV). Despite its importance, the amount and spatial distribution of water within the MTZ, and its impact on IPV, are poorly constrained. Here we use a series of plate tectonic reconstructions to estimate rates and positions of water injection into the MTZ by subducted slabs during the past 400 Myr. This allows us to construct maps of heterogeneous MTZ hydration, which we then compare to IPV locations since 200 Ma. We find a statistically significant correlation between wet regions of the MTZ and locations of IPV at the surface, but only if water remains stored in the MTZ for periods of 30-100 Myr after being carried there by slabs. We find that 42-68% of IPV is underlain by wet MTZ, with higher correlations associated with longer MTZ residence time, slower slab sinking rates, and longer time periods between MTZ hydration and IPV eruption. The correlation is highest during the Jurassic, when more extensive slab interaction with the MTZ caused a wider area of the MTZ to become hydrated. Parts of the MTZ near the western Pacific, southern Africa, and western Europe, have remained dry by avoiding wet slabs. Hydrous upwellings rising from the MTZ, some driven by interactions with subducting slabs, may be responsible for IPV rising from wet MTZ regions.

Plain Language Summary

Minerals within Earth's interior may hold several oceans of water. Most of this water is stored within the mantle transition zone (MTZ), a layer that lies between 410 and 670 km depth. It is carried there by subducted "slabs", which are tectonic plates that have descended into the mantle. We used plate tectonic reconstructions to determine the locations and rates of water transport into the MTZ by slabs during the past 400 million years. This exercise allows us to construct maps of water storage within Earth's MTZ. These maps suggest that more than a third of the MTZ is likely hydrated today, and even greater areas were likely hydrated in the past. We also found that "intraplate" volcanism erupting away from tectonic plate boundaries tends to preferentially occur above these "wet" areas of the MTZ, especially if water is assumed to remain in the MTZ for long periods of time. Based on this correlation, we hypothesize that intraplate volcanism is promoted above wet regions of the MTZ, where hydrous upwellings increase the tendency of rocks in the upper mantle to melt and form magma that can erupt.

1. Introduction

Water exchange between the Earth's surface and interior is facilitated by active plate tectonic processes, primarily subduction and mid-ocean ridge volcanism (Figure 1) [e.g., *Bodnar et al.*, 2013; *Thompson*, 1992]. The process of transporting water from the surface into the mantle through subduction is known as regassing (Figure 1) **Error! Reference source not found.**[*Rüpke et al.*, 2004; *Syracuse et al.*, 2010], and regassing rates depend on many parameters that control the thermal structure of subducting slabs. Old and fast slabs have a greater capacity to transport water to great depths (ca. >200 km) than young and warm, slowly subducting slabs [*Thompson*, 1992; *van Keken et al.*, 2011]. This is mainly because old and thick lithosphere that subducts rapidly can maintain a cold interior for longer, which allows hydrous phases within the slab to remain stable to greater depths. Water that reaches the mantle transition zone (MTZ, between 410 and 670 km depth) can be stored there for long periods within the minerals ringwoodite and wadsleyite [*Hirschmann*, 2006], especially if the slab's passage through the MTZ is slowed by slab stagnation, deformation, or horizontal deflection [*Komabayashi and Omori*, 2006; *Kuritani et al.*, 2011; *Ohtani et al.*, 2018; *Suetsugu et al.*, 2006]. The presence of water within the MTZ has been confirmed by examination of mineral inclusions within sublithospheric diamonds [*Pearson et al.*, 2014; *Shirey et al.*, 2021; *Wirth et al.*, 2007], and isotopic evidence suggests that MTZ water may have been recycled from the surface environment [*Xing et al.*, 2024]. Because slabs on Earth exhibit a diversity of thicknesses and descent rates, the subduction-mediated processes that deliver water to the deep mantle (> 200 km, beyond extraction by volcanic arcs, see Figure 1) are highly variable in space and time [e.g., *Karlsen et al.*, 2019; *van Keken et al.*, 2011]. Thus, even though the MTZ may hold even more water than Earth's surface environment [e.g., *Nestola and Smyth*, 2016], the distribution of this water within the MTZ may be highly heterogeneous [*Peslier et al.*, 2017].

Characterizing the water content of the transition zone is important because it can help us to understand Earth's deep mantle water cycle, which regulates mantle convection [e.g., *Karato*, 2011], upper mantle rheology [e.g., *Ramirez et al.*, 2022], volcanic processes [e.g., *Yang and Faccenda*, 2020], Phanerozoic sea level [e.g., *Karlsen et al.*, 2019], and Earth's thermal evolution [e.g., *Crowley et al.*, 2011]. However, detecting variations in MTZ hydration has proven difficult because such variations do not significantly influence seismic wave speeds [*Schulze et al.*, 2018]. Instead, variations in water content have been inferred from observations of transition zone thickness [*Houser*, 2016; *Meier et al.*, 2009; *Suetsugu et al.*, 2006], seismic anisotropy [*Chang and Ferreira*, 2019], and electrical conductivity [*Huang et al.*, 2005; *Karato*, 2011; *Kelbert et al.*, 2009]. The interpretation of such variations in terms of hydration heterogeneity may be complicated by the presence of other heterogeneities (e.g., temperature or composition [e.g., *Ramirez et al.*, 2022]), as suggested by conflicting inferences of mostly wet [*Kelbert et al.*, 2009] or mostly dry [*Chang and Ferreira*, 2019] conditions near subducting slabs. Overall, the magnitude and distribution of water in the Earth's interior, both today and in the geologic past, remain poorly quantified and mapped [*Hirschmann*, 2006].

One indicator of a hydrated MTZ may be intraplate volcanism (IPV), defined as volcanism occurring within the interiors of tectonic plates, i.e., away from plate boundaries. Although it is often associated with mantle plumes, IPV may also result from a variety of local processes including shear-driven upwelling [e.g., *Ballmer et al.*, 2015; *Conrad et al.*, 2011], lithospheric deformation [e.g., *Valentine and Hirano*, 2010], and sublithospheric convective instability [e.g., *Ballmer et al.*, 2010; *King and Ritsema*, 2000]. All of these IPV mechanisms rely on decompression melting beneath the lithosphere [e.g., *Aivazpourporgou et al.*, 2015; *Hernlund et al.*, 2008], which can be enhanced if the solidus temperature is depressed by the presence of water [*Katz et al.*, 2003]. Indeed, some IPV has been associated with melting above a locally hydrated mantle transition zone [*Kuritani et al.*, 2019; *Long et al.*, 2019; *Motoki and Ballmer*, 2015; *Wang et al.*, 2015; *Yang and Faccenda*, 2020]. Such a connection could be explained by upwelling of, or slab interaction with, an MTZ water reservoir [*Kuritani et al.*, 2011]. Because minerals found above the MTZ can bear less water, an upward flux of hydrated mantle above the 410 km discontinuity would result in hydrous melting [*Wang et al.*, 2015] and possibly the transport of melt to erupt at the surface [*Komabayashi and Omori*, 2006; *Kuritani et al.*, 2019] (Figure 1). This link between IPV and a hydrated MTZ may explain Cenozoic IPV in Northeast China [*Kuritani et al.*, 2011; *Yang and Faccenda*, 2020], where the Pacific slab has stagnated in the MTZ for more than 30 Myr [*Long et al.*, 2019].

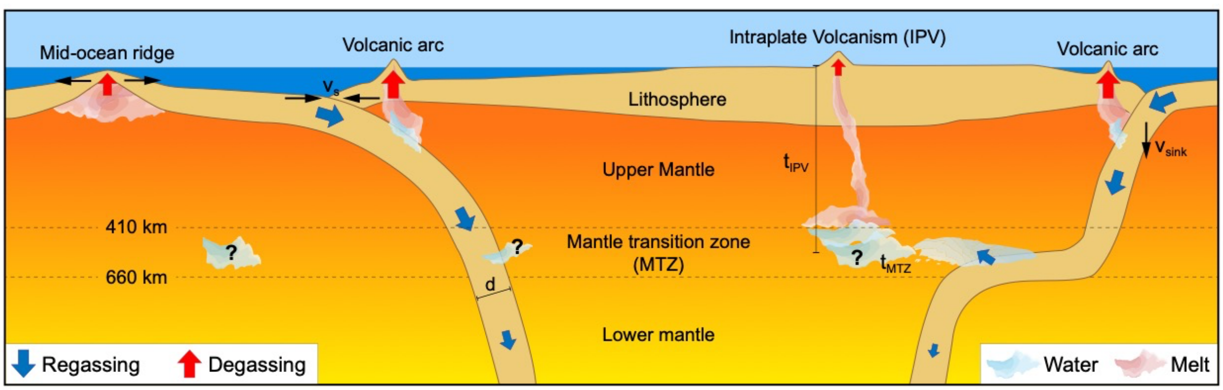

Figure 1. Schematic of the deep Earth water cycle. *Water exchange between Earth's surface and Earth's deep interior is controlled by plate tectonics. Degassing releases water to the surface at spreading ridges, arc volcanoes, and through intraplate volcanism (IPV). Regassing transports water back into the deep mantle via subduction, with velocity v_{sink}. Most of a slab's initial water is released in the mantle wedge, where it triggers partial melting and is degassed to the surface through arc volcanism. The remaining water is transported beyond the arc and can be released within the mantle transition zone (MTZ), where slabs often stagnate. More water reaches the MTZ for subduction zones with a larger convergence velocity (v_s) and a greater slab age (which determines the slab thickness, d). Water is plausibly stable within the MTZ for a significant time (t_{MTZ}), possibly even after the slab has continued sinking into the lower mantle. The hydrous MTZ may induce hydrous upwelling, melting, and subsequent IPV that is not plume-related [e.g., Yang and Faccenda, 2020]. Eruptions at intraplate locations above water-rich parts of the MTZ could occur after an unknown delay period (t_{IPV}) following MTZ hydration.*

In this study we look for a possible connection between continental intraplate volcanism and hydrated regions of the mantle transition zone. So far, this link has only been investigated through the lens of specific case studies conducted at a regional scale [e.g., *Kuritani et al.*, 2011; *Yang and Faccenda*, 2020]. Here we use global plate tectonic reconstructions to predict patterns of heterogeneous water storage in the MTZ during the past 400 Myr (section 2.1). We then test to see if IPV locations, inferred from a geochemical database (2.2), preferentially erupt above the more hydrated regions of the MTZ (2.3). Because our estimates of both subduction history and IPV patterns are imperfect, especially for earlier times, we examine geographical correlations between MTZ hydration state and IPV eruption locations from a statistical perspective (section 3). This allows us to use statistical correlation methods to quantify any inferred link between IPV locations and the hydrated MTZ (section 4).

2. Methods

Because the mechanisms for both hydration of the MTZ and eruption of IPV at the surface are poorly understood, we develop several alternative models of MTZ hydration based on values of key parameters whose true values are unknown. We then compare patterns of predicted MTZ hydration with IPV locations, compiled as described below, in order to discover any links between them.

2.1 Mapping hydrated regions in the mantle

To construct maps of the hydrated portions of the MTZ, we used the global plate tectonic model of *Matthews et al.* [2016], with corrections for the Pacific described by *Torsvik et al.* [2019]. The plate model is constructed upon a mantle-based absolute reference frame, extends from 410 Ma to present-day, and is accompanied by seafloor ages computed by *Karlsen et al.* [2021] (Figure 2, left column). For each 1 Myr time step, we extract the coordinates of the subduction zone segments, as well as their convergence velocity (v_s), length (L_s), and slab age (τ), all of which vary spatially and with time during the past 400 Myr (Figure S1).We use these parameters to estimate the flux of water into the deep mantle for each subduction zone segment at each time step, following the parametrization of *Karlsen et al.* [2019] (see Supplementary Text S1). The resulting regassing rates vary along and among Earth's different subduction zones (Figure 2, left column), and global rates of net regassing into the deep mantle exhibit significant temporal variations (Figure S1e). These regassing rates can be used to reconstruct hydration patterns in the MTZ as a function of time. The simplest way to do this is to integrate the historical water flux (HWF) for surface subduction zones for a chosen period of time. HWF is computed for each reconstruction time as the mass of along-trench regassed water that could have accumulated within the MTZ. By assuming an accumulation period (for example, 100 Myr) we can predict patterns of MTZ hydration that can be compared to the observed history of IPV (Figure 2, right column).

We convert integrations of HWF (units of Tg/m, right column of Figure 2) into maps of MTZ hydration density (kg of water per square km of MTZ), which are more useful for comparing to IPV eruptions. For this, we express regassing fluxes at subduction zones on a mesh of 10094 nodes distributed with relatively uniform spacing (~225 km at the surface) over a sphere (Figure S2). This results in a mapping of the water flux from the surface into the mantle at a particular time. We assume that water subducts vertically downward into the mantle beneath trench segment midpoints with a constant sinking velocity v_{sink}, which allows us to translate the water flux map to a specific mantle depth. Average upper mantle sinking velocities of 1-4 cm/yr [*van der Meer et al.*, 2018], 1.5-6.0 cm/yr [*Domeier et al.*, 2016], 5-7 cm/yr [*Goes et al.*, 2011], and 10 cm/yr [*Bercovici and Karato*, 2003] have been suggested. Here we employ v_{sink} as an unknown parameter and examine values in the range of 1-9 cm/yr above 660 km depth.

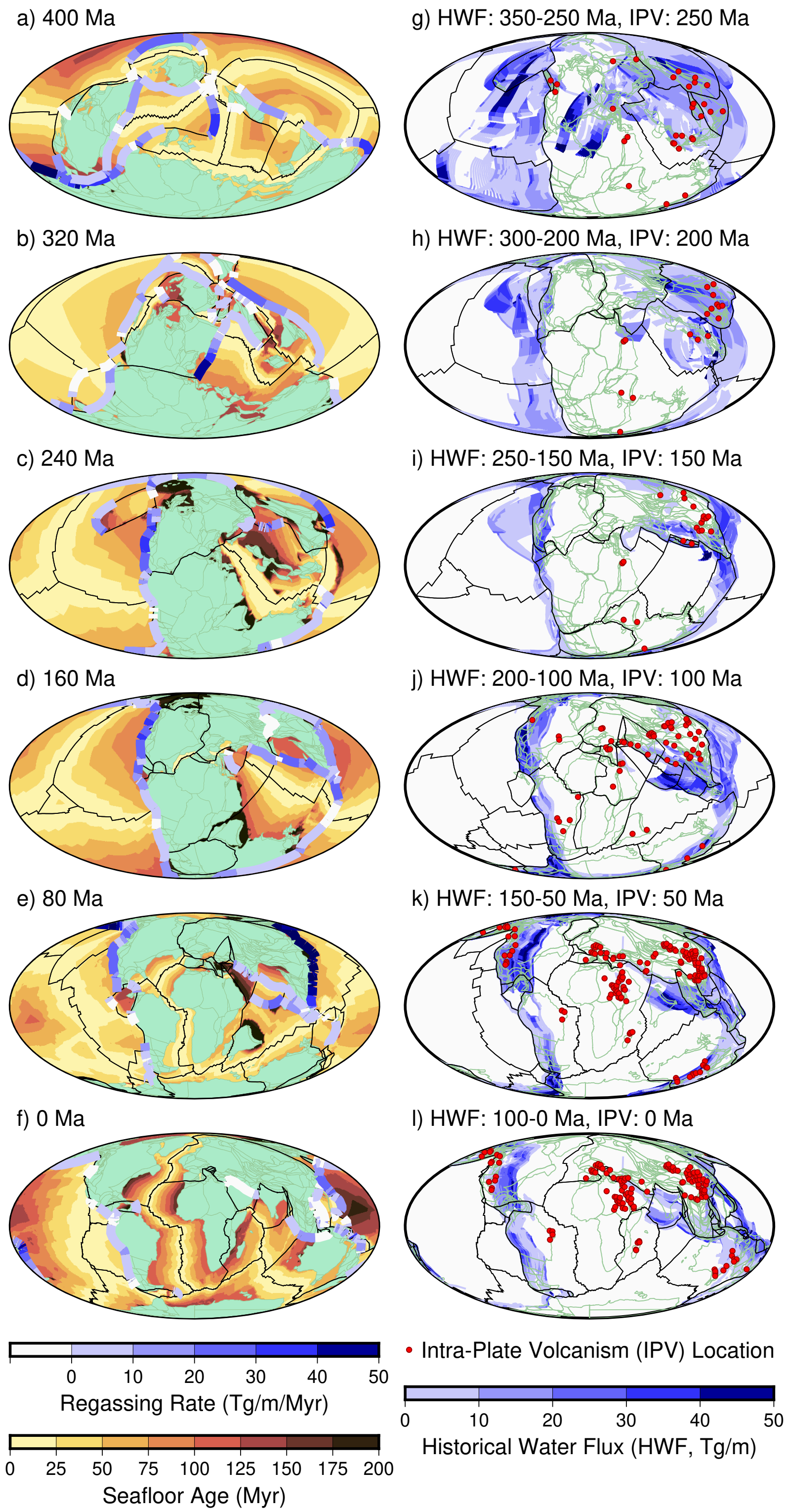

Figure 2. Regassing rates for subduction zone segments (left column) *colored according to the amount of water per unit length of subduction zone segment (per Myr) at (a) 400 Ma, (b) 320 Ma, (c) 240 Ma, (d) 160 Ma, (e) 80 Ma, and (f) 0 Ma (present day). Subduction zone segments that do not contribute to the deep mantle water flux (because they are too warm or subduct too slowly) are displayed as white segments. Also shown for context are reconstructed seafloor ages (colors in oceanic regions, from Karlsen et al. [2019]), plate boundaries (black lines), and continental blocks (green regions).* ***Historical water flux (HWF) and intraplate volcanism (IPV) eruption locations (right column)****, shown at (g) 250 Ma, (h) 200 Ma, (i) 150 Ma, (j) 100 Ma, (k) 50 Ma, and (l) 0 Ma (present-day). Here HWF (colors) represents the mass of water (per unit trench length) that has been injected into the deep mantle by subduction during the previous 100 Myrs (plotted using 1 Myr intervals). Our analysis compares representations of HWF to observed IPV locations, which are shown by red circles (see text for how IPV locations are determined).*

As they encounter the lower mantle, slabs are thought to slow down (e.g., *Butterworth* *et al.* [2014] estimated sinking rates of 1.3 cm/yr in the lower mantle), a process that may already begin in the MTZ. Some slabs appear to penetrate through the MTZ, whereas other slabs stagnate there for a period of time (Figure 1; [*Goes et al.*, 2017]). For scenarios of slab stagnation, we apply a sinking rate of 0 cm/yr at the 660 km discontinuity for a time t_{MTZ}, which we refer to as the MTZ residence time. We note that the effective MTZ residence time may be longer than the time that slabs actually stagnate in the MTZ. This is because any water that is released from a stagnating slab can be stored within wadsleyite and ringwoodite in the MTZ, even after the slab itself has moved deeper into the mantle. Because the duration of slab stagnation is unknown, we employ t_{MTZ} as another unknown parameter and examine plausible scenarios that include t_{MTZ} of 0, 30, and 100 Myr, after which we remove this water from the MTZ. We also consider an "infinite" end member case, named $t_{MTZ}=\infty$, in which all regassed water that reaches the MTZ stays there until the end of the simulation.

Within the upper mantle, water in the slab may migrate or diffuse into surrounding minerals [*Demouchy and Bolfan-Casanova*, 2016], which increases the lateral reach of the subducted water. In addition to diffusion, the location of the water may deviate from the surface location of the trench because slabs dip and deform as they descend, and may drift horizontally if they stagnate [*Goes et al.*, 2017]. To account for the lateral movement of water after subduction as well as uncertainties related to reconstructed subduction zone locations, we distribute water from each subduction zone segment into the *N* closest neighbor mesh points that surround the segment midpoint, with closer points getting more water (Supplementary Text S2). We use *N*=10, which distributes the water within a radius of about 390 km of the segment midpoint (Figure S2) and is consistent with slow diffusion processes [*Demouchy and Bolfan-Casanova*, 2016]. Sensitivity experiments show that increasing *N* has only a modest effect on the water distribution within the MTZ (Supplementary Text S2). Instead, the lateral coverage of water in the MTZ is more closely related to slab stagnation (section 3.2 below). This is because slab stagnation retains water within the MTZ while subduction locations, and thus MTZ injection points, dictate its distribution. The largest control on the lateral extent of MTZ hydration is thus exerted by changing the MTZ residence time t_{MTZ}.

2.2 Location of continental intraplate volcanism

To identify locations of continental intraplate volcanism (IPV), we selected all onshore basalts classified as "Intraplate Volcanism" from the GEOROC (Geochemistry of Rocks of the Oceans and Continents, https://georoc.eu/) database [*Lehnert et al.*, 2000] with assigned eruption ages within the most recent 250 Myr. The choice of 250 Myr allows time for the tectonic reconstruction to populate the MTZ with water following the start of the tectonic reconstruction at 410 Ma. We did not include sites classified as ocean islands, as a majority of those sites are likely related to mantle plumes, and thus a deep mantle source below the MTZ. Furthermore, oceanic intraplate volcanism is continually erased by subduction, which makes the oceanic IPV record uneven and incomplete. Although some of the continental IPV points in the dataset are likely also related to plumes, we did not attempt to remove such points because it is difficult to distinguish plume-associated IPV from other IPV. Thus, we used the database "as-is" (downloaded on November 16, 2021) to avoid selection bias. Importantly, the database shows only the present-day location of IPV, but due to plate motions most of these sites were in a different location at the time of their emplacement. Therefore, we computed the original position of each IPV point according to the same plate reconstruction model used to estimate the water flux to the mantle [*Matthews et al.*, 2016; *Torsvik et al.*, 2019], yielding maps of IPV locations for past times (Figure 2, right column). For comparison to MTZ hydration, we also filtered the data to exclude duplicate points and merged clustered points to mitigate oversampling (Supplementary Text S3; Figure S3).

2.3 Occurrence of IPV above wet or dry mantle

Having developed models for MTZ hydration and IPV eruption as a function of time and space (Figure 2); we now seek to determine if there exists any meaningful correlation between them. We might anticipate a delay period (t_{IPV}) between the charging of the MTZ with water and the eruption of IPV at the surface, associated with the ascent rate of hydrous upwellings from the MTZ and the time for melt to penetrate the lithosphere. Previous studies suggest IPV delay periods of ~12 Myr [*Yang and Faccenda*, 2020], tens of Myr [*Motoki and Ballmer*, 2015], and 10-30 Myr [*Long et al.*, 2019]. Therefore, we compare IPV maps (e.g., Fig. 2, right column) with MTZ hydration maps that are older by t_{IPV} delay periods of 0, 10, 20, 30, and 50 Myr.

We interpolate our MTZ hydration models (section 2.1) to determine the concentration of water in the MTZ beneath each IPV point. To identify regions of the MTZ where subducted water may have accumulated, we choose a threshold of $0.5 \cdot 10^9$ kg/km^2 to define the 'wet mantle transition zone', while values below this cutoff are designated as 'dry'. This threshold, which equates to a layer of water 0.5 m thick distributed within the 250 km thickness of the MTZ, lies just above the minimum non-zero MTZ water content in our maps (e.g., Figure 3). It is ~20 times smaller than 0.001 wt % water, which is the cutoff used by *Zhang et al.* [2022] to define the "dry" MTZ. We use a more generous definition of the "wet" MTZ because we want to include all regions of the MTZ that may have retained any water from slabs. We note that even small amounts of water can cause reduced viscosity and melting of mantle rocks [*Drewitt et al.*, 2022; *Hirschmann*, 2006; *Luth*, 2003; *Wright*, 2006]. We use a wet/dry distinction, rather than using water concentrations directly, because we only consider the presence of IPV; we do not consider eruption volumes in our analysis. Furthermore, we do not know how much water is needed to promote IPV, and other factors that may affect the formation of IPV are poorly constrained. Therefore, we do not attach extra importance to IPV occurrences above higher MTZ water concentrations.

For a quantitative measure of the degree of correlation between IPV and wet MTZ, we determined the percentage of volcanic eruptions located vertically above "wet" MTZ. We compared IPV and wet MTZ in this way for each 1 Myr time increment in the past, and averaged over the period 250-0 Ma.

3 Distribution of water in the mantle transition zone and comparison to IPV

We compare predictive maps of MTZ water content with the changing locations of IPV through the past 250 Myr. We start by examining a reference scenario based on specific choices for t_{MTZ}, v_{sink}, and t_{IPV}. By adjusting these parameters, we develop alternative models for the timing of MTZ hydration, which we test against observed IPV patterns for t_{MTZ}, v_{sink}, and t_{IPV}.

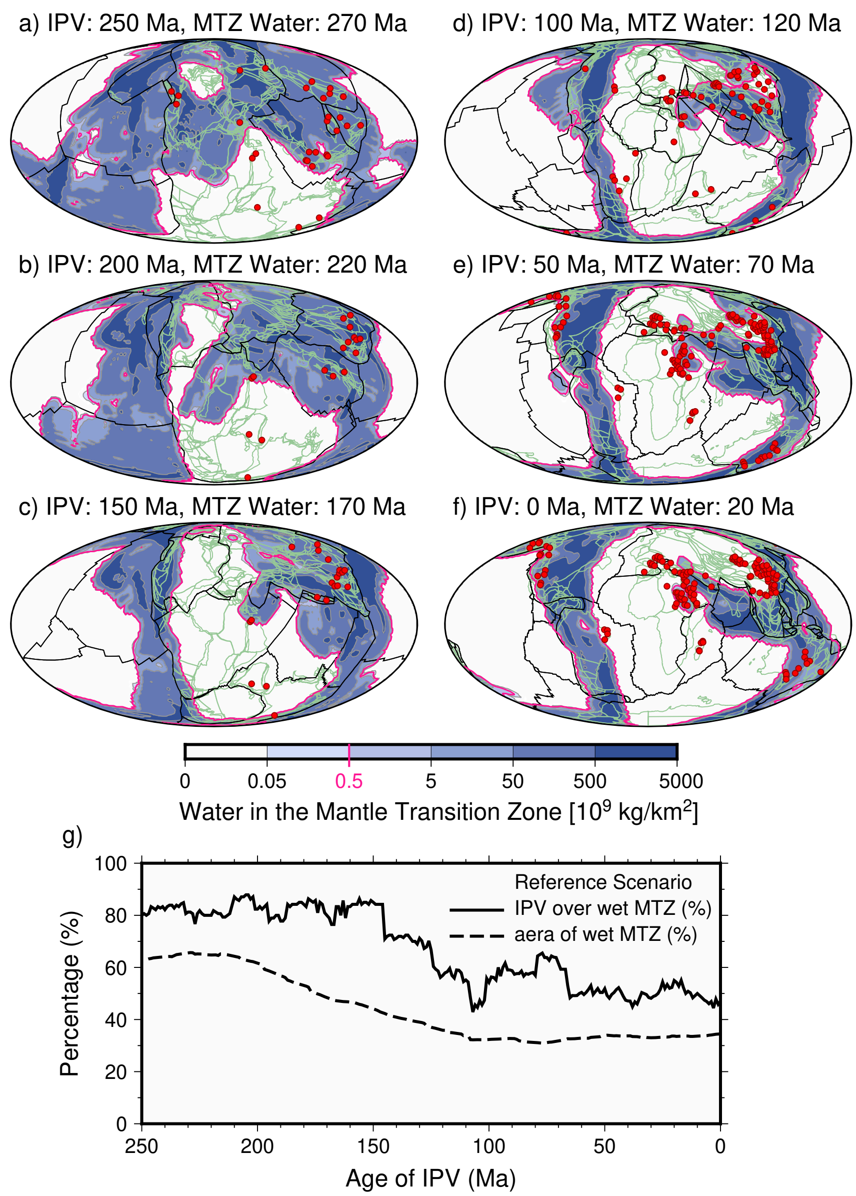

Figure 3. Comparison of IPV locations to the MTZ water distribution, for the reference scenario. *(a-f) Predictions of the water distribution in the mantle transition zone (colors) and locations of active intraplate volcanism (IPV, red points), for times between the present-day (a) and 250 Ma (f), with reconstructed coastlines (green lines) and plate boundaries (black lines). The reference scenario shown here assumes that water has a residence time of* $t_{MTZ} = 100$ *Myr in the MTZ, a slab sinking velocity of* $v_{sink} = 3$ *cm/yr, and a* $t_{IPV} = 20$ *Myr delay before IPV eruption. (g) Percentage of IPV locations that lie above wet MTZ (defined as* $\geq 0.5 \cdot 10^9$ *kg/km*^{2}*, pink contour in a-f) for this reference scenario (solid line). Shown for comparison is the fraction of the reference grid area that is covered by hydrated (rather than dry) MTZ regions (dashed line).*

3.1 The reference scenario

For our reference scenario, we apply a sinking rate of $v_{sink} = 3$ cm/yr, an MTZ water residence time of $t_{MTZ} = 100$ Myr, and an IPV delay period of $t_{IPV} = 20$ Myr. This model predicts that at 20 Ma (Figure 3f) the hydrated portion of the MTZ extended across regions of the mantle transition zone beneath present-day South and North America, the western Pacific and eastern Asia, and beneath India and some of the Middle East. This hydrated MTZ reflects patterns of Cenozoic subduction, which is expected given that slabs sinking at 3 cm/yr will reach the MTZ after only 15-20 Myr. Because subduction migrates slowly, this same geographical pattern has persisted since the Cretaceous (Figures 3d to 3f), with about one third of the MTZ being hydrated since 120 Ma (Figure 3g). Before the Cretaceous, the hydrated part of the MTZ covered a larger area, exceeding 60% of the MTZ area during 200-250 Ma (Figure 3g). However, much of the wet MTZ was only weakly hydrated during the Jurassic and earlier (Figures 3a and 3b), reflecting slower regassing rates prior to a peak at ~130 Ma [*Karlsen et al.*, 2019]. The area of the wet

MTZ was greater during these earlier periods because of faster trench migration rates in the tectonic reconstruction prior to ~250 Ma, perhaps resulting from ocean basin closure during supercontinent assembly [*Young et al.*, 2019].

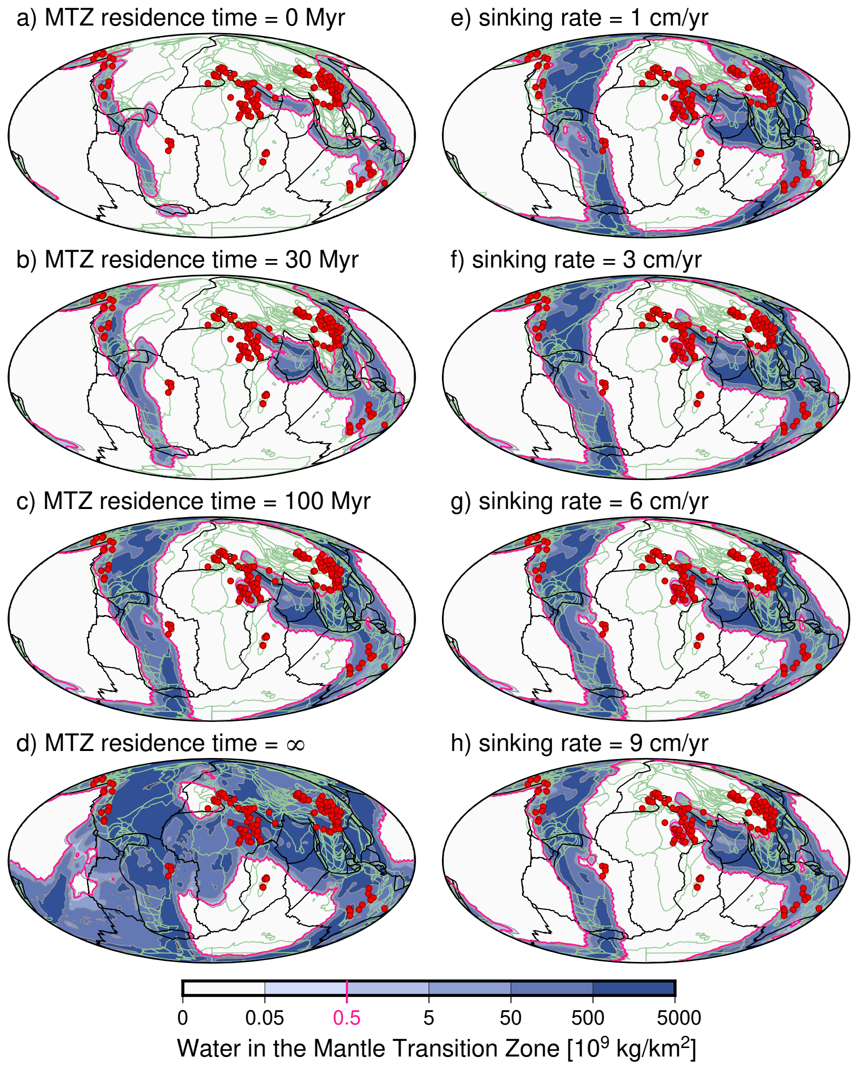

Figure 4. Effect of varying MTZ water residence time and slab sinking rates. Predictions of the water distribution in the mantle transition zone (MTZ) at 20 Ma for (a-d) varying MTZ residence time t_{MTZ} (assuming v_{sink} = 3 cm/yr and t_{IPV} = 20 Myr) and (e-h) varying slab sinking rate v_{sink} (assuming t_{MTZ} = 100 Myr and t_{IPV} = 20 Myr). Shown for all plots are continental outlines (green lines), plate boundaries (black lines) and active intraplate volcanism (IPV) locations (red dots) at 0 Ma. The pink contour outlines the wet MTZ (defined as $\geq 0.5 \cdot 10^9$ kg/km^2).

We compare the 132 IPV samples for the present day (0 Ma) to the MTZ at 20 Ma, accounting for the t_{IPV} = 20 Myr delay time before eruption (Figure 3f). We find that 47% of the 132 IPV samples overlie a wet MTZ (Figure 3g). Many of these "wet" IPV locations lie in eastern Asia and western North America (Figure 3f). Several points are located above MTZ that is only slightly hydrated, and some "dry" IPV locations are positioned near the edge of hydrated MTZ. Allowing for faster lateral spreading of hydration, or permitting greater MTZ water residence time, would likely result in more IPV overlaying wet MTZ. This correlation of IPV with the edges of the wet MTZ persists for IPV at 50 Ma (compared to the MTZ at 70 Ma, Figure 3e) and earlier in the Cretaceous, during which ~40-50% of IPV is underlain by wet MTZ (Figure 3g). The correspondence between IPV and wet MTZ is higher at 250 and 200 Ma (Figures 3a and 3b), with more than ~80% of IPV underlain by MTZ that was wet 20 Myr prior (Figure 3g). This higher percentage likely results from a more geographically expansive wet MTZ before the Cretaceous. Across 0 to 250 Ma, an average of 66.6% of the IPV locations reconstruct above MTZ that was wet 20 Myr before eruption.

3.2 MTZ water residence time

By varying the MTZ residence time t_{MTZ}, we show that the volume of water in the MTZ increases with increased residence time, as expected (Figure 4a-d). At 20 Ma (the time that is compared to present-day IPV for t_{IPV} = 20 Myr), wet conditions extend across only ~13% of the MTZ area for t_{MTZ} = 0 Myr (water sinks through the MTZ in less than 9 Myr at 3 cm/yr), but across ~74% if the MTZ if the residence time is unlimited ($t_{MTZ}=\infty$) (Figure 5a). This trend is also evident for past times (e.g., at 100 and 200 Ma, Figure S4), where wet conditions tend to quickly "fill up" the MTZ for longer MTZ residence times. Because of this greater area-coverage of wet conditions, we find that more IPV locations lie above hydrated MTZ for longer residence times (Figure 5a). As for the reference scenario (Figure 3a), the fraction of IPV underlain by wet MTZ is nearly always larger than the area fraction of the wet MTZ (Figure 5a). This means that IPV locations preferentially occur above the wet MTZ.

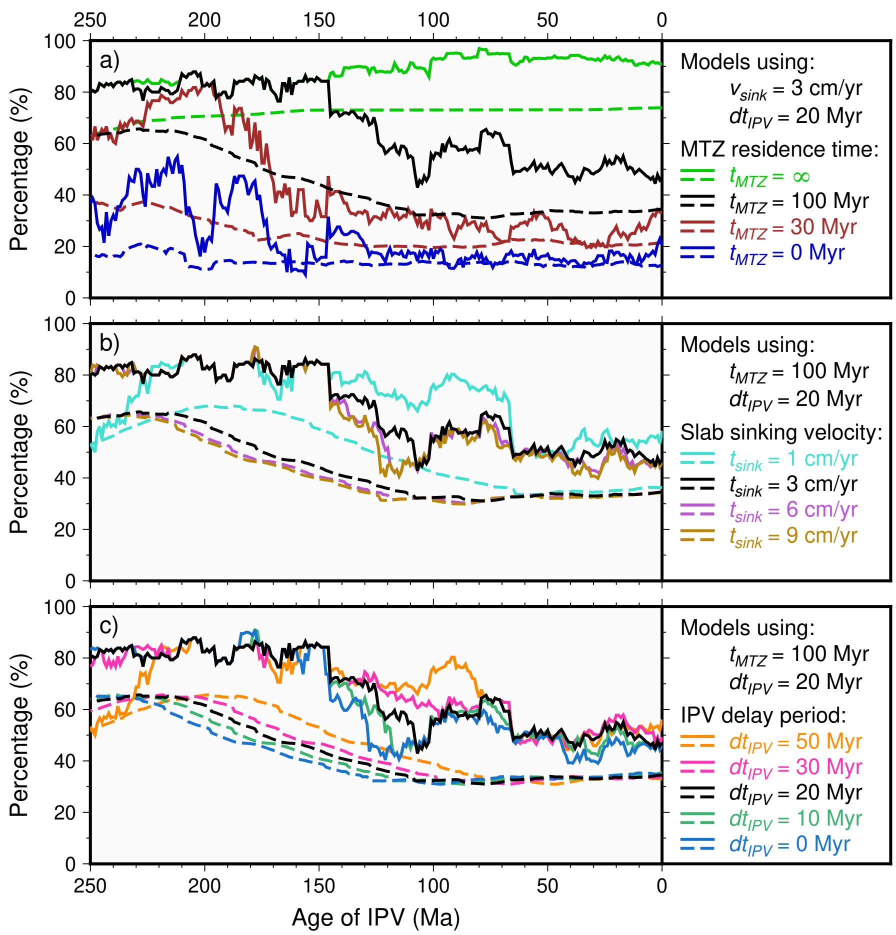

Figure 5. Comparisons of intraplate volcanism (IPV) locations with the hydrated mantle transition zone (MTZ) for different scenarios. *Shown is the fraction of IPV locations positioned above wet MTZ (solid lines) and the representative fraction of grid area covered by wet (rather than dry) MTZ regions (dashed lines). (a) Varying MTZ residence times (t_{MTZ}) for scenarios with v_{sink} = 3 cm/yr and t_{IPV} = 20 Myr. (b) Varying slab sinking rates (v_{sink}) for scenarios with t_{MTZ} =100 Myr and t_{IPV} = 20 Myr. (c) Varying IPV delay periods (t_{IPV}) for scenarios with t_{MTZ} =100 Myr and v_{sink} = 3 cm/yr. The black lines reproduce the lines in Figure 3g, i.e., the reference scenario.*

3.3 Slab sinking rate

The slab sinking rate v_{sink} determines the time it takes for subducted water to reach the MTZ, and a slower sinking rate extends the time that water spends within MTZ. However, varying the slab sinking rate between 1 and 9 cm/yr does not significantly change the predicted water distribution within the MTZ (Figure 4e-h), although more water is present within the MTZ for slower sinking rates (at 20 Ma, 36.3% of the MTZ is wet for $v_{sink} = 1$ cm/yr compared to 34.4% for $v_{sink} = 9$ cm/yr). Across the past 250 Myr (Figure 5b), a slow 1 cm/yr slab sinking rate results in a slightly better average match between IPV and wet MTZ than for faster sinking rates.

3.4 IPV delay period

Because the wet MTZ changes only gradually with time (e.g., Figure 3), the IPV delay period t_{IPV}, even one as long as 30 or 50 Myr, does not significantly affect the correlation between hydrated regions of the MTZ and IPV eruptions (Figure 5c). This parameter (t_{IPV}) also does not affect the area of wet MTZ (dashed lines, Figure 5c), but effectively shifts it to younger ages (rightward in Figure 5c) because IPV eruption locations are compared to the MTZ at the (older) time before the delay.

4 Statistical significance of correlations

We use a statistical approach to determine whether the observed correlations between IPV locations and the hydrated regions in the MTZ can be considered significant. Specifically, we seek to test the null-hypothesis that the observed correlation can be explained as a chance occurrence. To achieve this, we compute the observed fit against a set of randomly perturbed trials and conduct a one-tailed test. This allows us to determine the p-value, which is a measure of the likelihood of obtaining a correlation as large or larger than the observed value by random chance, i.e., the null-hypothesis. A small p-value (typically $p \leq 0.05$) suggests that the null-hypothesis is unlikely, and can be rejected.

To develop a set of random comparisons from which to derive an empirical distribution, we randomly re-oriented (see Supplementary Text S4) the simulated MTZ water grid (as constructed for a given set of model parameters). To obtain a statistically significant sample, we re-oriented each MTZ water grid 10^4 times, applying the same re-orientation for each time-step (within 0-250 Ma) of a given model. We then determine the fraction of IPV locations (which remain unperturbed) occurring above wet MTZ for each randomly re-oriented MTZ grid (see examples in Figure S5), and find the average over 250 million years, as before. Applying this procedure to the 10^4 different random rotations, we construct a distribution of wet IPV fractions for these "randomized wet MTZ scenarios" (Figure 6). The p-value is given as the fraction of this empirical distribution with a correlation between IPV and wet MTZ that is in excess of the observed value. If less than 5% of the random re-orientations yield a higher wet IPV fraction ($p < 0.05$ in Figure 6), then we can conclude that the observed correlation between IPV locations and the wet MTZ is not random. Note that the p-value that we obtain using this method is independent of the number of volcanism samples and is valid even if IPV sampling is incomplete [*Conrad et al.*, 2011]. This approach was applied to all scenarios of this study to determine which correlations may be statistically significant.

For the reference scenario, 66.6% of IPV locations since 250 Ma are underlain by wet MTZ (Figure 5a and Section 3.1). Of the 10^4 re-oriented MTZ water grids, only 3.9% produced correlations greater than 66.6% (Figure 6, top). This corresponds to a p-value of 0.039, which satisfies $p < 0.05$ and means that we can reject the null hypothesis (that the observed correlation between IPV and wet MTZ is a chance occurrence) at the 95% confidence level. Applying the same procedure to the other models for the wet MTZ, in which we vary t_{MTZ}, v_{sink}, and t_{IPV}, (Figure 6), we find that several other models exhibit correlations that are statistically significant at the 95% confidence level ($p \leq 0.05$). In particular, we find that changes to the reference scenario with t_{MTZ} of 30 to 100 Myr, v_{sink} of 3 cm/yr or more, and t_{IPV} between 10 and 30 Myr, can all produce correlations that are statistically significant at the 95% confidence level (Figure 6). These statistical tests suggest that there could be a meaningful link between the occurrence of IPV and hydrated regions of the MTZ, at least for the reference scenario and a range of models that are similar to it.

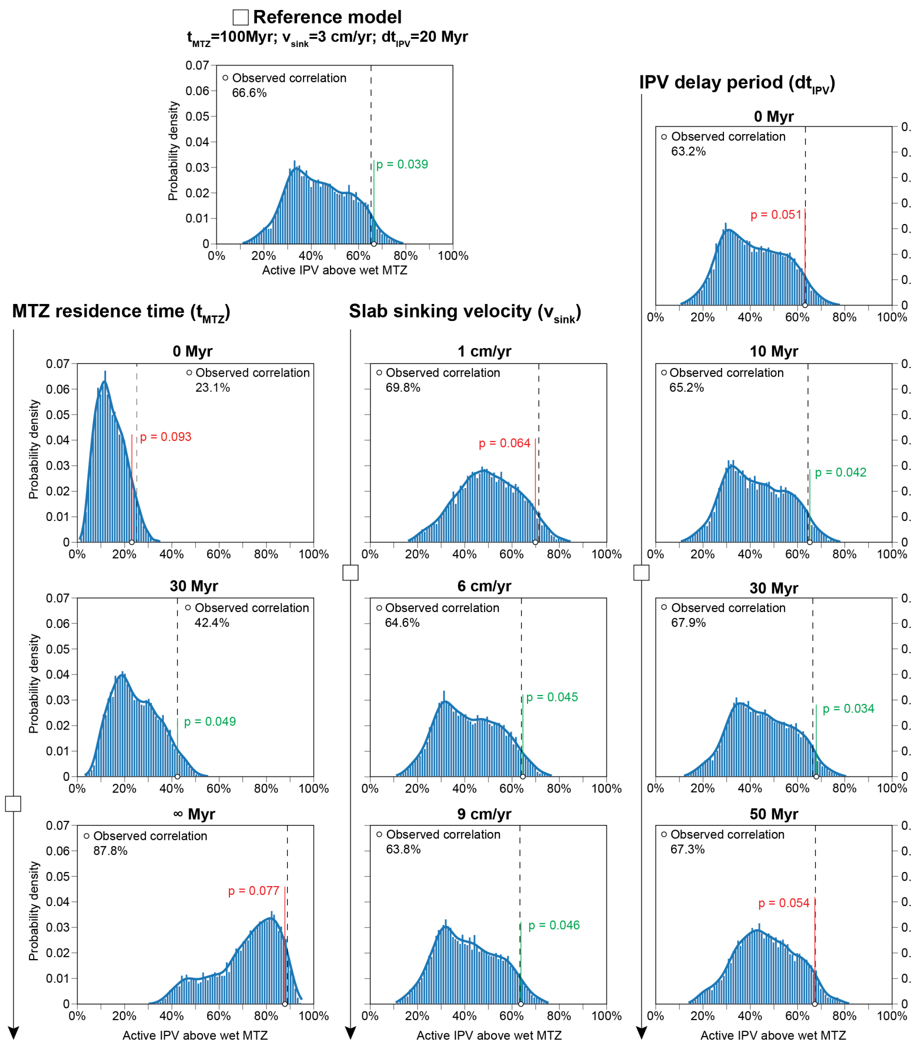

Figure 6. Distribution of correlations between IPV locations and randomly-oriented wet MTZ for the various models of this study. *The scenarios examined include the reference scenario (top left, marked with □), and variations to it involving the MTZ residence time (t_{MTZ}, left column), the slab sinking rate (v_{sink}, middle) and the IPV delay period (t_{IPV}, right). Here the observed correlation between IPV locations and wet MTZ is drawn with a black dashed line (observed value given in black). The percentage of the distribution with a correlation larger than observed is given by the p value, with p < 0.05 (shown by green labels) indicating that the observed correlation between IPV and wet MTZ is unlikely to result from random chance. In the remaining cases (p > 0.05, red labels) the null hypothesis cannot be rejected at the 95% confidence level.*

5 Discussion

We have estimated the rates and volumes of water transport into the deep mantle from modeled subduction fluxes based on plate tectonic reconstructions spanning 400 Myr. From these, we quantified the spatial heterogeneity of water in the MTZ. We find a statistically significant correlation between predicted hydrous regions of the MTZ and the locations of intraplate volcanism. Models with a statistical significance above the 95% confidence level display a match with continental intraplate volcanism between 42-68% (Figure 6), suggesting that over the past 250 Myr a large fraction of IPV has occurred above wet regions of the mantle.

We considered multiple models as defined by choices for several different variables that control the distribution of subducted water in the MTZ. We find that the alignment of IPV locations with the wet MTZ in our models depends significantly on the MTZ water residence time (t_{MTZ}), while the slab sinking rate and IPV delay time are less important. We find a p-value ≤ 0.05 for models with t_{MTZ} between 30 and 100 Myr (Figure 6). Outside of this range, shorter MTZ residence times (e.g., 0 Myr) do not generate enough MTZ hydration to explain IPV at a level that is statistically significant, while longer MTZ residence times (e.g., ∞ case) add water to so much of the MTZ that even randomly-placed IPV locations are likely to sit above wet MTZ. This suggests that the temporary stagnation of slabs at the 660 km discontinuity, for periods of ~30 Myr or more, is crucial for MTZ hydration, and this hydration provides opportunities for generating IPV.

The fact that different choices of slab sinking rate and IPV delay time do not significantly affect correlations between IPV and wet MTZ, except for their most extreme values, suggests that these parameters are not significantly important to their linkage. We did observe a poor correlation (and less statistical significance) for the slowest sinking rate of 1 cm/yr (Figure 6); this indicates that a slow upper mantle sinking rate is not by itself sufficient to produce patterns of wet MTZ that are sufficiently correlated to IPV. Instead, it seems that stalling in the MTZ for ~30-100 Myr is necessary. Concerning the IPV delay period, the most statistically-significant result is for a delay period of 30 Myr (Figure 6), which supports the expectation of a nonzero IPV delay period because hydrous melt must be created, ascend to the asthenosphere, and travel through the lithosphere, to cause volcanic eruptions. However, the timing of these processes is still poorly understood and more research is needed to constrain the process of IPV generation by hydrous melt.

5.1 Implications of a correlation between IPV and wet MTZ

Establishing that IPV patterns correlate with hydrous MTZ regions supports the widely recognized hypothesis that water is transported to the MTZ by subducting slabs [*Bodnar et al.*, 2013; *Kelbert et al.*, 2009; *Magni et al.*, 2014; *Thompson*, 1992; *van Keken et al.*, 2011], and consequently generates spatial and temporal mantle heterogeneity [*Peslier et al.*, 2017]. This also suggests that tectonic reconstruction models are a valuable tool for exploring and estimating this heterogeneity. Generally, the MTZ water distribution over the period investigated (0-250 Ma) reflects continuous hydration of particular regions with a long history of subduction. Many of these regions are overlain by IPV (e.g., Figure 3). Such a link between a locally hydrated mantle transition zone and volcanism far from plate boundaries has been suggested by previous studies that mainly focused on a regional scale, for example the Cenozoic IPV in Northeast China

[*Kuritani et al.*, 2011; *Yang and Faccenda*, 2020]. Our study confirms this link, but globally and in a statistical sense, for IPV that erupted during the past 250 Myr.

Upwelling from hydrated parts of the MTZ, and the subsequent generation of melting and IPV eruption, may be a complicated process involving multiple geodynamic processes. For example, hydrous upwelling itself may require multiple subduction events to first saturate the MTZ and then to trigger upwelling flow of hydrated mantle [*Kuritani et al.*, 2011; *Yang and Faccenda*, 2020]. Therefore, although the presence of water in the MTZ is likely to promote IPV, it must do so in conjunction with mantle processes that operate on MTZ heterogeneity over time, including several that draw the mantle above stagnant slabs upward [*Kameyama and Nishioka*, 2012; *Kelbert et al.*, 2009; *Long et al.*, 2019]. Once hydrated rocks are in the asthenosphere, other processes such as shear-driven upwelling [e.g., *Ballmer et al.*, 2015; *Conrad et al.*, 2011], lithospheric deformation [e.g., *Valentine and Hirano*, 2010], and small-scale convection [e.g., *Ballmer et al.*, 2010; *King and Ritsema*, 2000] may be important to produce localized melting and eruption to the surface. Although we do not directly include such secondary processes within our models, we indirectly account for them when using large values of t_{MTZ} and t_{IPV}, for which we obtain the largest correlations between IPV and wet MTZ.

Among the parameters we consider, the strongest control appears to be exerted by the MTZ water residence time (t_{MTZ}), which implies that slab stagnation is important to MTZ hydration. The extra time that stagnating slabs spend in the MTZ may provide opportunities for incorporation of subducted water into the hydrous reservoirs of the MTZ [e.g., *Kuritani et al.*, 2011], which we have now associated with IPV at the surface. Storage of this water in the MTZ, even if temporary, removes water from the Earth's surface reservoirs, decreasing sea level [e.g., *Karlsen et al.*, 2019]. The presence of this water within the MTZ minerals of ringwoodite and wadsleyite may also be important for reducing MTZ viscosity toward observed values [*Fei et al.*, 2017], affecting global mantle flow patterns [e.g., *Karato*, 2011] and Earth's long-term thermal evolution [e.g., *Crowley et al.*, 2011]. Water loss from the MTZ may occur as mantle flow brings hydrated minerals across the upper [*Andrault and Bolfan-Casanova*, 2022] or lower [*Schmandt et al.*, 2014] boundaries of the MTZ. The addition of water to the assemblage of nominally anhydrous minerals in these regions results in melting, and the melt likely percolates upward [*Ohtani et al.*, 2018]. Melt that forms above the MTZ eventually reaches the asthenosphere, and can be erupted by IPV [*Andrault and Bolfan-Casanova*, 2022], as discussed above. Melt forming below the MTZ may also percolate upward, re-hydrating the MTZ [*Schmandt et al.*, 2014], but some water likely remains stored within lower mantle bridgmanite, and continues downward [*Walter*, 2021]. Our results suggest that these processes overall lead to an average longevity of water in the MTZ of order 30-100 Myr, with much uncertainty.

It is notable that we observe better agreement between IPV locations and the hydrated MTZ for earlier times (~125-250 Ma). This is the opposite of what we might expect given that the uncertainties on both the plate reconstruction and the IPV database generally increase with time. However, large regassing rates early in the tectonic reconstruction (before 320 Ma, Figure S1e) and rapid trench migration [*Young et al.*, 2019] may have hydrated significant parts of the MTZ during the period ~400-200 Ma. The storage of this water in the MTZ for periods of up to 100 Myr (large MTZ residence times) may have induced IPV across a wide region during the first part of our analysis (~250-150 Ma). Alternatively, the decreasing number of IPV samples for older times (Figure S3c) may indicate sampling bias. If this bias involves preferential sampling of eruptions that are larger in magnitude (greater eruptive volume), then it is possible that such larger-scale IPV events are more likely to be related to melting of hydrous upper mantle, which should produce greater melt volumes. By contrast, the database of recent IPV may over-represent small-scale events that are less likely to be related to wet MTZ.

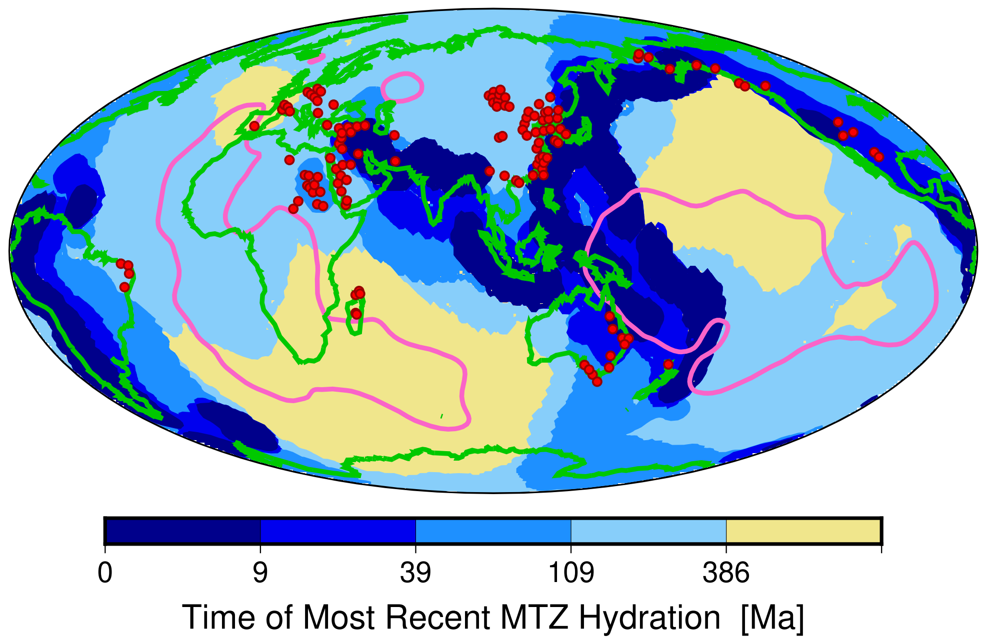

Figure 7. Map of the time of the most recent MTZ hydration *(colors), as compared to current IPV volcanism (red dots), continental locations (green lines), and LLSVP locations at the base of the mantle (pink lines). Here we assume a slab sinking rate of 3 cm/yr, and plot colors based on the ages of interaction of these slabs with the MTZ model for the four different choices of t_{MTZ} that we examined. We note that three major areas of the MTZ (regions with yellow colors, near western Europe, southern Africa and the western Pacific) have not interacted with hydrated slabs in the past 400 Myr.*

5.2 Dry regions of the mantle transition zone

The water mapped in this study is transported to the MTZ through subduction. Therefore, areas that have remained far from subduction zones throughout the considered period should be relatively dry (Figure 7), unless ancient water has remained stable for longer periods (> 400 Myr) or water has been transported into these regions by other means. This suggests that the MTZ beneath the Indian Ocean, Southeast Africa, the South Atlantic Ocean, large parts of the North Pacific Ocean, and a modest area below western Europe have remained dry for the past 400 Myr, and should be dry today. We note that there is relatively little IPV above the "dry" areas, although many of these regions are covered by oceanic lithosphere, where we have not considered IPV. These "dry" areas away from subduction zones roughly correspond to areas of persistent and stable broad-scale upwelling in the mantle [*Conrad et al.*, 2013], which represents a return-flow from subduction downwelling occurring around these areas [*Shephard et al.*, 2017]. Intraplate volcanism has been identified within these regions away from subduction, but it has been mostly associated with deep mantle plumes (e.g., Hawaii). Plume-induced intraplate volcanism has been associated with the edges of the Large Low Shear Velocity Provinces (LLSVPs) at the base of the mantle, which form away from subduction zones [*Torsvik et al.*, 2016]. Some of the IPV identified within the "dry" areas of the MTZ (Figure 7) may thus be associated with plumes rising from the deep mantle.

Because the presence of water tends to reduce viscosity of the MTZ [*Fei et al.*, 2017], these dry regions should have a larger viscosity than the wetter areas that surround them. This increased viscosity may be partially offset by decreased viscosity associated with mantle upwelling and increased temperatures associated with these regions away from subduction zones [*Conrad et al.*, 2013]. However, if these dry regions of the MTZ are indeed stiffer than their surroundings, then mantle deformation should preferentially occur in the wetter areas, affecting upper mantle flow patterns [*Ramirez et al.*, 2023]. Indeed, subduction-related deformation has tended to occur away from these potentially dry areas above the LLSVPs [*Shephard et al.*, 2017], preventing hydration of these areas of the MTZ (Figure 7) and perhaps stabilizing large-scale mantle flow patterns [*Conrad et al.*, 2013]. A dry MTZ may also exert an important influence on rates of glacial isostatic adjustment (GIA), which includes the solid Earth's viscous response to episodes of deglaciation. Indeed, one of the dry regions in our models is predicted to extend beneath East Antarctica (Figure 7). Here, elevated upper mantle viscosities have been shown to slow rates of uplift in response to past (and future) deglaciation there, with important implications for sea level change [*Gomez et al.*, 2024].

5.3 Limitations

Uncertainties in the generated MTZ water grids are partly linked to and controlled by the underlying plate tectonic model [*Karlsen et al.*, 2021; *Karlsen et al.*, 2020; *Matthews et al.*, 2016; *Torsvik et al.*, 2019], which becomes increasingly poorly constrained for older time periods. We assume vertical subduction, which has been suggested to be reasonable for mapping subducted slabs [*Domeier et al.*, 2016], but does not account for lateral deflections or slab stagnations that may affect the MTZ water content. Thus, we have had to introduce additional parameterizations, such as the threshold for wet MTZ and the number of nearest neighbors used to spread the water laterally. These choices are poorly constrained and affect the MTZ water distribution and its link to IPV. We argue that the statistical approach used here (section 4) allows us to overcome this uncertainty by looking for overall correlations, even weak ones, based on "best guess" choices for some of these unknown parameters. Of course, this means that our predictive maps of MTZ hydration include a significant degree of uncertainty.

We have shown that one of the most important parameters is the MTZ residence time, which is related to slab stagnation. However, not all slabs behave the same way; some may stagnate for different amounts of time in the MTZ while other slabs may subduct directly through it. Therefore, our assumption of using one constant value of MTZ residence time per model is a significant simplification. A more detailed mapping of wet and dry regions in the mantle transition zone (Figure 7) could be constructed by considering these different behaviors for each slab. It could be possible to infer slab topology from tomographic models for recent times, but would unfortunately be difficult, if not impossible, to do so for past times. However, if we assume that there is indeed a link between wet MTZ and the occurrence of IPV, one could use the location and ages of IPV to speculate on the temporal and spatial variations of the MTZ hydration state back in time.

Our hypothesis testing using IPV locations may be limited by the geochemical dataset that we used. In particular, we are heavily dependent on the classifications of volcanism within the GEOROC database [*Lehnert et al.*, 2000]; we only considered intraplate volcanism with basaltic compositions. We did not attempt to remove plume-related events, except that we only considered continental locations. Thus, there are an unknown number of "IPV" samples in our dataset that have a plume source, e.g., the Afar plume below the African rift. The ability to remove these points is hindered by limited knowledge of past plume events; known hotspot volcanism was therefore not filtered out to preserve consistency.

One of the greatest uncertainties of the statistical test is our choice of $0.5 \cdot 10^9$ kg/km^2 for the threshold between wet and dry MTZ. A low threshold is reasonable as even a tiny amount of water can generate melt production if the mantle conditions are close to the solidus, although more water is needed to produce melting in colder regions [*Karato et al.*, 2020; *Katz et al.*, 2003] and buoyant hydrous upwelling requires significant hydration [*Yang and Faccenda*, 2020]. However, other mechanisms that require less water may help to link the wet MTZ to IPV. We note that the specific choice of a threshold may not be too important, because the area covered by water values between 0.05 and $5 \cdot 10^9$ kg/km^2 is rather small compared to the overall "wet" area (Figures 3 and 4). However, choosing a larger value for the threshold may impact the match percentages between the wet MTZ and IPV locations, and the statistical significance of these matches. Alternatively, it could be useful to investigate correlations between the degree of MTZ hydration and the volumes of IPV. However, the IPV database that we are using does not include constraints on volumes of IPV, and such constraints are difficult to obtain anyway. Overall, an improved understanding of the mechanism behind non-hotspot IPV is needed to choose a more appropriate value for this threshold.

6 Conclusions

Our study suggests that the mantle transition zone (MTZ, 410-660 km) is likely to be heterogeneously hydrated, with wetter regions beneath areas with a long history of subduction, and regions away from subduction remaining dry (Figure 7). To show this, we created maps of the spatial and temporal heterogeneity of water storage in the mantle transition zone (e.g., Figure 3), based on tectonic reconstructions for the last 400 Ma and the assumption that subduction transports water downward into the MTZ. Using these maps, we discovered a positive correlation between wet regions of the MTZ and locations of intraplate volcanism (IPV) at the surface (Figure 5), and we demonstrated that this correlation is statistically significant (Figure 6). In particular, we showed that water must reside in the MTZ for long periods (timescales of 30 to 100 Myr) in order for the hydrous regions of the MTZ to be positively correlated with IPV in a statistically significant way (>95% confidence that the association is not random). This is because slab stagnation at the MTZ allows for slab dehydration and water accumulation in the surrounding MTZ rocks. We also found that a time delay of 10 to 30 Myr between MTZ hydration and IPV eruption tends to produce better correlations. This long MTZ residence time and long IPV delay time suggest that significant time and perhaps multiple subduction events are required to hydrate the MTZ, mobilize the hydrated mantle to generate melt, and transport this melt upwards for eruption at the surface.

The MTZ water distribution, as characterized by our predictive maps (Figures 3 and 4) is mostly dictated by tectonic patterns of subduction at the surface, including the plate convergence rate, trench migration rate, and subducting plate age for subduction zones around the world [*Karlsen et al.*, 2019]. We find that the area fraction of wet MTZ was likely greater in the past

(>150 Ma), because of a more extensive subduction network that migrated more quickly [*Young et al.*, 2019]. The extent of hydration also depends critically on the residence time of water in the MTZ, as controlled by slab stagnation [*Komabayashi and Omori*, 2006; *Kuritani et al.*, 2011] and possible MTZ rehydration [*Schmandt et al.*, 2014] as water is released from dehydrating lower mantle slabs [*Walter*, 2021]. Also important are processes that generate upwelling and upwards water transport from the hydrous regions of the MTZ [*Kuritani et al.*, 2019; *Wang et al.*, 2015; *Yang and Faccenda*, 2020], leading to melting beneath the lithosphere [*Long et al.*, 2019; *Motoki and Ballmer*, 2015] and eruption at the surface.

Beyond the important implications for IPV that we have detailed here, a heterogeneously hydrated MTZ should also be viscously heterogeneous [*Fei et al.*, 2017]. This is important because MTZ viscosity controls rates of upper mantle flow [*Ramirez et al.*, 2023], planetary thermal evolution [*Crowley et al.*, 2011], and even recent deglaciation-induced solid earth uplift [*Gomez et al.*, 2024]. Thus, new comparisons between geophysical, geologic, and tectonic constraints on the hydration state of the MTZ, exemplified by our study, can help us to understand a variety of important geodynamic processes.

Open Research. The intraplate volcanism database is taken from the GEOROC (Geochemistry of Rocks of the Oceans and Continents, https://georoc.eu/) database, with data available from *Lehnert et al.* [2000]. Mapping of the hydrous regions of the mantle transition zone utilizes the GPlates software [*Müller et al.*, 2018], which can be accesses at https://www.gplates.org, and data from the global plate tectonic model of *Matthews et al.* [2016], corrections for the Pacific from *Torsvik et al.* [2019], and seafloor ages from *Karlsen et al.* [2021].

Acknowledgements. This work was partly supported by the Research Council of Norway via project 288449 (MAGPIE project) and via its Centres of Excellence scheme, project numbers 223272 (CEED) and 332523 (PHAB). We thank Krister Karlsen for valuable assistance with the regassing model, and Stephane Rondenay and Tobias Rolf for reviewing an early version of this manuscript.

References

Aivazpourporgou, S., S. Thiel, P. C. Hayman, L. N. Moresi, and G. Heinson (2015), Decompression melting driving intraplate volcanism in Australia: Evidence from magnetotelluric sounding, *Geophysical Research Letters*, *42*(2), 2014GL060088, doi:10.1002/2014GL060088.

Andrault, D., and N. Bolfan-Casanova (2022), Mantle rain toward the Earth's surface: A model for the internal cycle of water, *Physics of the Earth and Planetary Interiors*, *322*, 106815, doi:https://doi.org/10.1016/j.pepi.2021.106815.

Ballmer, M. D., C. P. Conrad, E. I. Smith, and R. Johnsen (2015), Intraplate volcanism at the edges of the Colorado Plateau sustained by a combination of triggered edge-driven convection and shear-driven upwelling, *Geochemistry, Geophysics, Geosystems*, *16*(2), 366-379, doi:10.1002/2014GC005641.

Ballmer, M. D., G. Ito, J. van Hunen, and P. J. Tackley (2010), Small-scale sublithospheric convection reconciles geochemistry and geochronology of 'Superplume' volcanism in the western and south Pacific, *Earth and Planetary Science Letters*, *290*(1–2), 224-232, doi:http://dx.doi.org/10.1016/j.epsl.2009.12.025.

Bercovici, D., and S.-i. Karato (2003), Whole-mantle convection and the transition-zone water filter, *Nature*, *425*(6953), 39-44, doi:10.1038/nature01918.

Bodnar, R. J., T. Azbej, S. P. Becker, C. Cannatelli, A. Fall, and M. J. Severs (2013), Whole Earth geohydrologic cycle, from the clouds to the core: The distribution of water in the dynamic Earth system, *Geological Society of America Special Papers*, *500*, 431-461, doi:10.1130/2013.2500(13).

Butterworth, N. P., A. S. Talsma, R. D. Müller, M. Seton, H. P. Bunge, B. S. A. Schuberth, G. E. Shephard, and C. Heine (2014), Geological, tomographic, kinematic and geodynamic constraints on the dynamics of sinking slabs, *Journal of Geodynamics*, *73*, 1-13, doi:https://doi.org/10.1016/j.jog.2013.10.006.

Chang, S.-J., and A. M. G. Ferreira (2019), Inference on Water Content in the Mantle Transition Zone Near Subducted Slabs From Anisotropy Tomography, *Geochemistry, Geophysics, Geosystems*, *20*(2), 1189-1201, doi:10.1029/2018gc008090.

Conrad, C. P., T. A. Bianco, E. I. Smith, and P. Wessel (2011), Patterns of intraplate volcanism controlled by asthenospheric shear, *Nature Geoscience*, *4*(5), 317-321, doi:10.1038/ngeo1111.

Conrad, C. P., B. Steinberger, and T. H. Torsvik (2013), Stability of active mantle upwelling revealed by net characteristics of plate tectonics, *Nature*, *498*(7455), 479-482, doi:10.1038/nature12203.

Crowley, J. W., M. Gérault, and R. J. O'Connell (2011), On the relative influence of heat and water transport on planetary dynamics, *Earth and Planetary Science Letters*, *310*(3–4), 380-388, doi:10.1016/j.epsl.2011.08.035.

Demouchy, S., and N. Bolfan-Casanova (2016), Distribution and transport of hydrogen in the lithospheric mantle: A review, *Lithos*, *240-243*, 402-425, doi:https://doi.org/10.1016/j.lithos.2015.11.012.

Domeier, M., P. V. Doubrovine, T. H. Torsvik, W. Spakman, and A. L. Bull (2016), Global correlation of lower mantle structure and past subduction, *Geophysical Research Letters*, *43*(10), 4945-4953, doi:10.1002/2016GL068827.

Drewitt, J. W. E., M. J. Walter, J. P. Brodholt, J. M. R. Muir, and O. T. Lord (2022), Hydrous silicate melts and the deep mantle H2O cycle, *Earth and Planetary Science Letters*, *581*, 117408, doi:https://doi.org/10.1016/j.epsl.2022.117408.

Fei, H., D. Yamazaki, M. Sakurai, N. Miyajima, H. Ohfuji, T. Katsura, and T. Yamamoto (2017), A nearly water-saturated mantle transition zone inferred from mineral viscosity, *Science Advances*, *3*(6), doi:10.1126/sciadv.1603024.

Goes, S., R. Agrusta, J. van Hunen, and F. Garel (2017), Subduction-transition zone interaction: A review, *Geopsphere*, *13*(7), 644-664, doi:10.1130/GES01476.1.

Goes, S., F. A. Capitanio, G. Morra, M. Seton, and D. Giardini (2011), Signatures of downgoing plate-buoyancy driven subduction in Cenozoic plate motions, *Physics of the Earth and Planetary Interiors*, *184*(1), 1-13, doi:https://doi.org/10.1016/j.pepi.2010.10.007.

Gomez, N., M. Yousefi, D. Pollard, R. M. DeConto, S. Sadai, A. Lloyd, A. Nyblade, D. A. Wiens, R. C. Aster, and T. Wilson (2024), The influence of realistic 3D mantle viscosity on Antarctica's contribution to future global sea levels, *Science Advances*, *10*(31), eadn1470, doi:doi:10.1126/sciadv.adn1470.

Hernlund, J. W., D. J. Stevenson, and P. J. Tackley (2008), Buoyant melting instabilities beneath extending lithosphere: 2. Linear analysis, *Journal of Geophysical Research: Solid Earth*, *113*(B4), doi:https://doi.org/10.1029/2006JB004863.

Hirschmann, M. M. (2006), Water, melting, and the deep earth H20 cycle, *Annual Review of Earth and Planetary Sciences*, *34*(1), 629-653, doi:10.1146/annurev.earth.34.031405.125211.

Houser, C. (2016), Global seismic data reveal little water in the mantle transition zone, *Earth and Planetary Science Letters*, *448*, 94-101, doi:http://dx.doi.org/10.1016/j.epsl.2016.04.018.

Huang, X., Y. Xu, and S.-i. Karato (2005), Water content in the transition zone from electrical conductivity of wadsleyite and ringwoodite, *Nature*, *434*(7034), 746-749, doi:10.1038/nature03426.

Kameyama, M., and R. Nishioka (2012), Generation of ascending flows in the Big Mantle Wedge (BMW) beneath northeast Asia induced by retreat and stagnation of subducted slab, *Geophysical Research Letters*, *39*(10), doi:https://doi.org/10.1029/2012GL051678.

Karato, S.-i. (2011), Water distribution across the mantle transition zone and its implications for global material circulation, *Earth and Planetary Science Letters*, *301*(3–4), 413-423, doi:10.1016/j.epsl.2010.11.038.

Karato, S.-i., B. Karki, and J. Park (2020), Deep mantle melting, global water circulation and its implications for the stability of the ocean mass, *Progress in Earth and Planetary Science*, *7*(1), 76, doi:10.1186/s40645-020-00379-3.

Karlsen, K. S., C. P. Conrad, M. Domeier, and R. G. Trønnes (2021), Spatiotemporal Variations in Surface Heat Loss Imply a Heterogeneous Mantle Cooling History, *Geophysical Research Letters*, *48*(6), e2020GL092119, doi:https://doi.org/10.1029/2020GL092119.

Karlsen, K. S., C. P. Conrad, and V. Magni (2019), Deep Water Cycling and Sea Level Change Since the Breakup of Pangea, *Geochemistry, Geophysics, Geosystems*, *20*(6), 2919-2935, doi:10.1029/2019GC008232.

Karlsen, K. S., M. Domeier, C. Gaina, and C. P. Conrad (2020), A tracer-based algorithm for automatic generation of seafloor age grids from plate tectonic reconstructions, *Computers & Geosciences*, *140*, 104508, doi:https://doi.org/10.1016/j.cageo.2020.104508.

Katz, R. F., M. Spiegelman, and C. H. Langmuir (2003), A new parameterization of hydrous mantle melting, *Geochemistry, Geophysics, Geosystems*, *4*(9), doi:https://doi.org/10.1029/2002GC000433.

Kelbert, A., A. Schultz, and G. Egbert (2009), Global electromagnetic induction constraints on transition-zone water content variations, *Nature*, *460*(7258), 1003-1006, doi:10.1038/nature08257.

King, S. D., and J. Ritsema (2000), African Hot Spot Volcanism: Small-Scale Convection in the Upper Mantle Beneath Cratons, *Science*, *290*(5494), 1137-1140, doi:10.1126/science.290.5494.1137.

Komabayashi, T., and S. Omori (2006), Internally consistent thermodynamic data set for dense hydrous magnesium silicates up to 35GPa, 1600°C: Implications for water circulation in the Earth's deep mantle, *Physics of the Earth and Planetary Interiors*, *156*(1), 89-107, doi:https://doi.org/10.1016/j.pepi.2006.02.002.

Kuritani, T., E. Ohtani, and J.-I. Kimura (2011), Intensive hydration of the mantle transition zone beneath China caused by ancient slab stagnation, *Nature Geosci*, *4*(10), 713-716, doi:http://dx.doi.org/10.1038/ngeo1250.

Kuritani, T., Q.-K. Xia, J.-I. Kimura, J. Liu, K. Shimizu, T. Ushikubo, D. Zhao, M. Nakagawa, and S. Yoshimura (2019), Buoyant hydrous mantle plume from the mantle transition zone, *Scientific Reports*, *9*(1), 6549, doi:10.1038/s41598-019-43103-y.

Lehnert, K., Y. Su, C. H. Langmuir, B. Sarbas, and U. Nohl (2000), A global geochemical database structure for rocks, *Geochemistry, Geophysics, Geosystems*, *1*(5), doi:https://doi.org/10.1029/1999GC000026.

Long, X., M. D. Ballmer, A. M.-C. Córdoba, and C.-F. Li (2019), Mantle Melting and Intraplate Volcanism Due to Self-Buoyant Hydrous Upwellings From the Stagnant Slab That Are Conveyed by Small-Scale Convection, *Geochemistry, Geophysics, Geosystems*, *20*(11), 4972-4997, doi:10.1029/2019gc008591.

Luth, R. W. (2003), 2.07 - Mantle Volatiles—Distribution and Consequences, in *Treatise on Geochemistry*, edited by H. D. Holland and K. K. Turekian, pp. 319-361, Pergamon, Oxford, doi:https://doi.org/10.1016/B0-08-043751-6/02124-1.

Magni, V., P. Bouilhol, and J. van Hunen (2014), Deep water recycling through time, *Geochemistry, Geophysics, Geosystems*, *15*(11), 4203-4216, doi:10.1002/2014GC005525.

Matthews, K. J., K. T. Maloney, S. Zahirovic, S. E. Williams, M. Seton, and R. D. Müller (2016), Global plate boundary evolution and kinematics since the late Paleozoic, *Global and Planetary Change*, *146*(Supplement C), 226-250, doi:10.1016/j.gloplacha.2016.10.002.

Meier, U., J. Trampert, and A. Curtis (2009), Global variations of temperature and water content in the mantle transition zone from higher mode surface waves, *Earth and Planetary Science Letters*, *282*(1), 91-101, doi:https://doi.org/10.1016/j.epsl.2009.03.004.

Motoki, M. H., and M. D. Ballmer (2015), Intraplate volcanism due to convective instability of stagnant slabs in the mantle transition zone, *Geochemistry, Geophysics, Geosystems*, *16*(2), 538-551, doi:https://doi.org/10.1002/2014GC005608.

Müller, R. D., J. Cannon, X. Qin, R. J. Watson, M. Gurnis, S. Williams, T. Pfaffelmoser, M. Seton, S. H. J. Russell, and S. Zahirovic (2018), GPlates: Building a Virtual Earth Through Deep Time, *Geochemistry, Geophysics, Geosystems*, *19*(7), 2243-2261, doi:doi:10.1029/2018GC007584.

Nestola, F., and J. R. Smyth (2016), Diamonds and water in the deep Earth: a new scenario, *International Geology Review*, *58*(3), 263-276, doi:10.1080/00206814.2015.1056758.

Ohtani, E., L. Yuan, I. Ohira, A. Shatskiy, and K. Litasov (2018), Fate of water transported into the deep mantle by slab subduction, *Journal of Asian Earth Sciences*, *167*, 2-10, doi:https://doi.org/10.1016/j.jseaes.2018.04.024.

Pearson, D. G., et al. (2014), Hydrous mantle transition zone indicated by ringwoodite included within diamond, *Nature*, *507*(7491), 221-224, doi:10.1038/nature13080.

Peslier, A. H., M. Schönbächler, H. Busemann, and S.-I. Karato (2017), Water in the Earth's Interior: Distribution and Origin, *Space Science Reviews*, *212*(1), 743-810, doi:10.1007/s11214-017-0387-z.

Ramirez, F. D. C., C. P. Conrad, and K. Selway (2023), Grain size reduction by plug flow in the wet oceanic upper mantle explains the asthenosphere's low seismic Q zone, *Earth and Planetary Science Letters*, *616*, 118232, doi:https://doi.org/10.1016/j.epsl.2023.118232.

Ramirez, F. D. C., K. Selway, C. P. Conrad, and C. Lithgow-Bertelloni (2022), Constraining Upper Mantle Viscosity Using Temperature and Water Content Inferred From Seismic and Magnetotelluric Data, *Journal of Geophysical Research: Solid Earth*, *127*(8), e2021JB023824, doi:https://doi.org/10.1029/2021JB023824.

Rüpke, L. H., J. P. Morgan, M. Hort, and J. A. D. Connolly (2004), Serpentine and the subduction zone water cycle, *Earth and Planetary Science Letters*, *223*(1–2), 17-34, doi:10.1016/j.epsl.2004.04.018.

Schmandt, B., S. D. Jacobsen, T. W. Becker, Z. Liu, and K. G. Dueker (2014), Dehydration melting at the top of the lower mantle, *Science*, *344*(6189), 1265-1268, doi:10.1126/science.1253358.

Schulze, K., H. Marquardt, T. Kawazoe, T. Boffa Ballaran, C. McCammon, M. Koch-Müller, A. Kurnosov, and K. Marquardt (2018), Seismically invisible water in Earth's transition zone?, *Earth and Planetary Science Letters*, *498*, 9-16, doi:https://doi.org/10.1016/j.epsl.2018.06.021.

Shephard, G. E., K. J. Matthews, K. Hosseini, and M. Domeier (2017), On the consistency of seismically imaged lower mantle slabs, *Scientific Reports*, *7*(1), 10976, doi:10.1038/s41598-017-11039-w.

Shirey, S. B., L. S. Wagner, M. J. Walter, D. G. Pearson, and P. E. van Keken (2021), Slab Transport of Fluids to Deep Focus Earthquake Depths—Thermal Modeling Constraints and Evidence From Diamonds, *AGU Advances*, *2*(2), e2020AV000304, doi:https://doi.org/10.1029/2020AV000304.

Suetsugu, D., T. Inoue, A. Yamada, D. Zhao, and M. Obayashi (2006), Towards Mapping the Three-Dimensional Distribution of Water in the Transition Zone from P-Velocity Tomography and 660-Km Discontinuity Depths, in *Earth's Deep Water Cycle*, edited, pp. 237-249, doi:https://doi.org/10.1029/168GM18.

Syracuse, E. M., P. E. van Keken, and G. A. Abers (2010), The global range of subduction zone thermal models, *Physics of the Earth and Planetary Interiors*, *183*(1–2), 73-90, doi:http://dx.doi.org/10.1016/j.pepi.2010.02.004.

Thompson, A. B. (1992), Water in the Earth's upper mantle, *Nature*, *358*(6384), 295-302, doi:10.1038/358295a0.

Torsvik, T. H., B. Steinberger, L. D. Ashwal, P. V. Doubrovine, and R. G. Trønnes (2016), Earth evolution and dynamics—a tribute to Kevin Burke, *Canadian Journal of Earth Sciences*, *53*(11), 1073-1087, doi:10.1139/cjes-2015-0228.

Torsvik, T. H., B. Steinberger, G. E. Shephard, P. V. Doubrovine, C. Gaina, M. Domeier, C. P. Conrad, and W. W. Sager (2019), Pacific-Panthalassic Reconstructions: Overview, Errata and the Way Forward, *Geochemistry, Geophysics, Geosystems*, *20*(7), 3659-3689, doi:10.1029/2019gc008402.

Valentine, G. A., and N. Hirano (2010), Mechanisms of low-flux intraplate volcanic fields—Basin and Range (North America) and northwest Pacific Ocean, *Geology*, *38*(1), 55-58, doi:10.1130/g30427.1.

van der Meer, D. G., D. J. J. van Hinsbergen, and W. Spakman (2018), Atlas of the underworld: Slab remnants in the mantle, their sinking history, and a new outlook on lower mantle viscosity, *Tectonophysics*, *723*, 309-448, doi:https://doi.org/10.1016/j.tecto.2017.10.004.

van Keken, P. E., B. R. Hacker, E. M. Syracuse, and G. A. Abers (2011), Subduction factory: 4. Depth-dependent flux of H2O from subducting slabs worldwide, *J. Geophys. Res.*, *116*(B1), B01401, doi:10.1029/2010jb007922.

Walter, M. J. (2021), Water transport to the core–mantle boundary, *National Science Review*, *8*(4), doi:10.1093/nsr/nwab007.

Wang, X.-C., S. A. Wilde, Q.-L. Li, and Y.-N. Yang (2015), Continental flood basalts derived from the hydrous mantle transition zone, *Nature Communications*, *6*(1), 7700, doi:10.1038/ncomms8700.

Wirth, R., C. Vollmer, F. Brenker, S. Matsyuk, and F. Kaminsky (2007), Inclusions of nanocrystalline hydrous aluminium silicate “Phase Egg” in superdeep diamonds from Juina (Mato Grosso State, Brazil), *Earth and Planetary Science Letters*, *259*(3), 384-399, doi:https://doi.org/10.1016/j.epsl.2007.04.041.

Wright, K. (2006), Atomistic Models of OH Defects in Nominally Anhydrous Minerals, *Reviews in Mineralogy and Geochemistry*, *62*(1), 67-83, doi:10.2138/rmg.2006.62.4.

Xing, K.-C., F. Wang, F.-Z. Teng, W.-L. Xu, Y.-N. Wang, D.-B. Yang, H.-L. Li, and Y.-C. Wang (2024), Potassium isotopic evidence for recycling of surface water into the mantle transition zone, *Nature Geoscience*, doi:10.1038/s41561-024-01452-y.

Yang, J., and M. Faccenda (2020), Intraplate volcanism originating from upwelling hydrous mantle transition zone, *Nature*, *579*(7797), 88-91, doi:10.1038/s41586-020-2045-y.

Young, A., N. Flament, K. Maloney, S. Williams, K. Matthews, S. Zahirovic, and R. D. Müller (2019), Global kinematics of tectonic plates and subduction zones since the late Paleozoic Era, *Geoscience Frontiers*, *10*(3), 989-1013, doi:https://doi.org/10.1016/j.gsf.2018.05.011.

Zhang, H., G. D. Egbert, and Q. Huang (2022), A relatively dry mantle transition zone revealed by geomagnetic diurnal variations, *Science Advances*, *8*(31), eabo3293, doi:doi:10.1126/sciadv.abo3293.

Hydrous regions of the mantle transition zone lie beneath areas of intraplate volcanism

Helene Wang[1,2], Valentina Magni[1,3], Clinton P. Conrad[1,4,*] and Mathew Domeier[1,4]

[1] Centre for Earth Evolution and Dynamics (CEED), University of Oslo, Oslo, Norway
[2] TGS, Oslo, Norway
[3] Norwegian Geotechnical Institute (NGI), Oslo, Norway
[4] Centre for Planetary Habitability (PHAB), University of Oslo, Oslo, Norway
[*] Corresponding author: Clinton P. Conrad (c.p.conrad@geo.uio.no)

Manuscript submitted to *Geochemistry, Geophysics, Geosystems,* September 2024

Key Points:

- We use tectonic reconstructions of subduction history to map the hydration state of the mantle transition zone (MTZ) for the past 400 Myr.
- We identify a statistically significant correlation between hydrated MTZ and intraplate volcanism (IPV) at the Earth's surface.
- Hydrated MTZ can explain IPV if subducted water stalls in the MTZ for ~100 Myr and hydrous upwelling induces sub-lithospheric melting.

Abstract

Great volumes of water are carried downward into the mantle transition zone (MTZ, 410-670 km depth) by subducting slabs. If this water is later drawn upward, the resulting mantle melting may generate intraplate volcanism (IPV). Despite its importance, the amount and spatial distribution of water within the MTZ, and its impact on IPV, are poorly constrained. Here we use a series of plate tectonic reconstructions to estimate rates and positions of water injection into the MTZ by subducted slabs during the past 400 Myr. This allows us to construct maps of heterogeneous MTZ hydration, which we then compare to IPV locations since 200 Ma. We find a statistically significant correlation between wet regions of the MTZ and locations of IPV at the surface, but only if water remains stored in the MTZ for periods of 30-100 Myr after being carried there by slabs. We find that 42-68% of IPV is underlain by wet MTZ, with higher correlations associated with longer MTZ residence time, slower slab sinking rates, and longer time periods between MTZ hydration and IPV eruption. The correlation is highest during the Jurassic, when more extensive slab interaction with the MTZ caused a wider area of the MTZ to become hydrated. Parts of the MTZ near the western Pacific, southern Africa, and western Europe, have remained dry by avoiding wet slabs. Hydrous upwellings rising from the MTZ, some driven by interactions with subducting slabs, may be responsible for IPV rising from wet MTZ regions.

Plain Language Summary

Minerals within Earth's interior may hold several oceans of water. Most of this water is stored within the mantle transition zone (MTZ), a layer that lies between 410 and 670 km depth. It is carried there by subducted "slabs", which are tectonic plates that have descended into the mantle. We used plate tectonic reconstructions to determine the locations and rates of water transport into the MTZ by slabs during the past 400 million years. This exercise allows us to construct maps of water storage within Earth's MTZ. These maps suggest that more than a third of the MTZ is likely hydrated today, and even greater areas were likely hydrated in the past. We also found that "intraplate" volcanism erupting away from tectonic plate boundaries tends to preferentially occur above these "wet" areas of the MTZ, especially if water is assumed to remain in the MTZ for long periods of time. Based on this correlation, we hypothesize that intraplate volcanism is promoted above wet regions of the MTZ, where hydrous upwellings increase the tendency of rocks in the upper mantle to melt and form magma that can erupt.

1. Introduction

Water exchange between the Earth's surface and interior is facilitated by active plate tectonic processes, primarily subduction and mid-ocean ridge volcanism (Figure 1) [e.g., *Bodnar et al.*, 2013; *Thompson*, 1992]. The process of transporting water from the surface into the mantle through subduction is known as regassing (Figure 1) **Error! Reference source not found.**[*Rüpke et al.*, 2004; *Syracuse et al.*, 2010], and regassing rates depend on many parameters that control the thermal structure of subducting slabs. Old and fast slabs have a greater capacity to transport water to great depths (ca. >200 km) than young and warm, slowly subducting slabs [*Thompson*, 1992; *van Keken et al.*, 2011]. This is mainly because old and thick lithosphere that subducts rapidly can maintain a cold interior for longer, which allows hydrous phases within the slab to remain stable to greater depths. Water that reaches the mantle transition zone (MTZ, between 410 and 670 km depth) can be stored there for long periods within the minerals ringwoodite and wadsleyite [*Hirschmann*, 2006], especially if the slab's passage through the MTZ is slowed by slab stagnation, deformation, or horizontal deflection [*Komabayashi and Omori*, 2006; *Kuritani et al.*, 2011; *Ohtani et al.*, 2018; *Suetsugu et al.*, 2006]. The presence of water within the MTZ has been confirmed by examination of mineral inclusions within sublithospheric diamonds [*Pearson et al.*, 2014; *Shirey et al.*, 2021; *Wirth et al.*, 2007], and isotopic evidence suggests that MTZ water may have been recycled from the surface environment [*Xing et al.*, 2024]. Because slabs on Earth exhibit a diversity of thicknesses and descent rates, the subduction-mediated processes that deliver water to the deep mantle (> 200 km, beyond extraction by volcanic arcs, see Figure 1) are highly variable in space and time [e.g., *Karlsen et al.*, 2019; *van Keken et al.*, 2011]. Thus, even though the MTZ may hold even more water than Earth's surface environment [e.g., *Nestola and Smyth*, 2016], the distribution of this water within the MTZ may be highly heterogeneous [*Peslier et al.*, 2017].

Characterizing the water content of the transition zone is important because it can help us to understand Earth's deep mantle water cycle, which regulates mantle convection [e.g., *Karato*, 2011], upper mantle rheology [e.g., *Ramirez et al.*, 2022], volcanic processes [e.g., *Yang and Faccenda*, 2020], Phanerozoic sea level [e.g., *Karlsen et al.*, 2019], and Earth's thermal evolution [e.g., *Crowley et al.*, 2011]. However, detecting variations in MTZ hydration has proven difficult because such variations do not significantly influence seismic wave speeds [*Schulze et al.*, 2018]. Instead, variations in water content have been inferred from observations of transition zone thickness [*Houser*, 2016; *Meier et al.*, 2009; *Suetsugu et al.*, 2006], seismic anisotropy [*Chang and Ferreira*, 2019], and electrical conductivity [*Huang et al.*, 2005; *Karato*, 2011; *Kelbert et al.*, 2009]. The interpretation of such variations in terms of hydration heterogeneity may be complicated by the presence of other heterogeneities (e.g., temperature or composition [e.g., *Ramirez et al.*, 2022]), as suggested by conflicting inferences of mostly wet [*Kelbert et al.*, 2009] or mostly dry [*Chang and Ferreira*, 2019] conditions near subducting slabs. Overall, the magnitude and distribution of water in the Earth's interior, both today and in the geologic past, remain poorly quantified and mapped [*Hirschmann*, 2006].

One indicator of a hydrated MTZ may be intraplate volcanism (IPV), defined as volcanism occurring within the interiors of tectonic plates, i.e., away from plate boundaries. Although it is often associated with mantle plumes, IPV may also result from a variety of local processes including shear-driven upwelling [e.g., *Ballmer et al.*, 2015; *Conrad et al.*, 2011], lithospheric deformation [e.g., *Valentine and Hirano*, 2010], and sublithospheric convective instability [e.g., *Ballmer et al.*, 2010; *King and Ritsema*, 2000]. All of these IPV mechanisms rely on decompression melting beneath the lithosphere [e.g., *Aivazpourporgou et al.*, 2015; *Hernlund et al.*, 2008], which can be enhanced if the solidus temperature is depressed by the presence of water [*Katz et al.*, 2003]. Indeed, some IPV has been associated with melting above a locally hydrated mantle transition zone [*Kuritani et al.*, 2019; *Long et al.*, 2019; *Motoki and Ballmer*, 2015; *Wang et al.*, 2015; *Yang and Faccenda*, 2020]. Such a connection could be explained by upwelling of, or slab interaction with, an MTZ water reservoir [*Kuritani et al.*, 2011]. Because minerals found above the MTZ can bear less water, an upward flux of hydrated mantle above the 410 km discontinuity would result in hydrous melting [*Wang et al.*, 2015] and possibly the transport of melt to erupt at the surface [*Komabayashi and Omori*, 2006; *Kuritani et al.*, 2019] (Figure 1). This link between IPV and a hydrated MTZ may explain Cenozoic IPV in Northeast China [*Kuritani et al.*, 2011; *Yang and Faccenda*, 2020], where the Pacific slab has stagnated in the MTZ for more than 30 Myr [*Long et al.*, 2019].

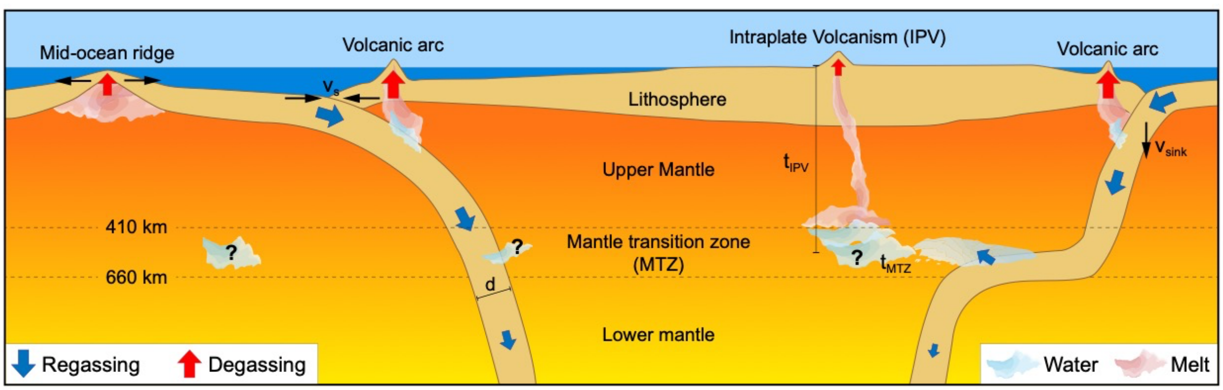

Figure 1. Schematic of the deep Earth water cycle. *Water exchange between Earth's surface and Earth's deep interior is controlled by plate tectonics. Degassing releases water to the surface at spreading ridges, arc volcanoes, and through intraplate volcanism (IPV). Regassing transports water back into the deep mantle via subduction, with velocity* v_{sink}*. Most of a slab's initial water is released in the mantle wedge, where it triggers partial melting and is degassed to the surface through arc volcanism. The remaining water is transported beyond the arc and can be released within the mantle transition zone (MTZ), where slabs often stagnate. More water reaches the MTZ for subduction zones with a larger convergence velocity (*v_s*) and a greater slab age (which determines the slab thickness, d). Water is plausibly stable within the MTZ for a significant time (*t_{MTZ}*), possibly even after the slab has continued sinking into the lower mantle. The hydrous MTZ may induce hydrous upwelling, melting, and subsequent IPV that is not plume-related [e.g., Yang and Faccenda, 2020]. Eruptions at intraplate locations above water-rich parts of the MTZ could occur after an unknown delay period (*t_{IPV}*) following MTZ hydration.*

In this study we look for a possible connection between continental intraplate volcanism and hydrated regions of the mantle transition zone. So far, this link has only been investigated through the lens of specific case studies conducted at a regional scale [e.g., *Kuritani et al.*, 2011; *Yang and Faccenda*, 2020]. Here we use global plate tectonic reconstructions to predict patterns of heterogeneous water storage in the MTZ during the past 400 Myr (section 2.1). We then test to see if IPV locations, inferred from a geochemical database (2.2), preferentially erupt above the more hydrated regions of the MTZ (2.3). Because our estimates of both subduction history and IPV patterns are imperfect, especially for earlier times, we examine geographical correlations between MTZ hydration state and IPV eruption locations from a statistical perspective (section 3). This allows us to use statistical correlation methods to quantify any inferred link between IPV locations and the hydrated MTZ (section 4).

2. Methods

Because the mechanisms for both hydration of the MTZ and eruption of IPV at the surface are poorly understood, we develop several alternative models of MTZ hydration based on values of key parameters whose true values are unknown. We then compare patterns of predicted MTZ hydration with IPV locations, compiled as described below, in order to discover any links between them.

2.1 Mapping hydrated regions in the mantle

To construct maps of the hydrated portions of the MTZ, we used the global plate tectonic model of *Matthews et al.* [2016], with corrections for the Pacific described by *Torsvik et al.* [2019]. The plate model is constructed upon a mantle-based absolute reference frame, extends from 410 Ma to present-day, and is accompanied by seafloor ages computed by *Karlsen et al.* [2021] (Figure 2, left column). For each 1 Myr time step, we extract the coordinates of the subduction zone segments, as well as their convergence velocity (v_s), length (L_s), and slab age (τ), all of which vary spatially and with time during the past 400 Myr (Figure S1).We use these parameters to estimate the flux of water into the deep mantle for each subduction zone segment at each time step, following the parametrization of *Karlsen et al.* [2019] (see Supplementary Text S1). The resulting regassing rates vary along and among Earth's different subduction zones (Figure 2, left column), and global rates of net regassing into the deep mantle exhibit significant temporal variations (Figure S1e). These regassing rates can be used to reconstruct hydration patterns in the MTZ as a function of time. The simplest way to do this is to integrate the historical water flux (HWF) for surface subduction zones for a chosen period of time. HWF is computed for each reconstruction time as the mass of along-trench regassed water that could have accumulated within the MTZ. By assuming an accumulation period (for example, 100 Myr) we can predict patterns of MTZ hydration that can be compared to the observed history of IPV (Figure 2, right column).

We convert integrations of HWF (units of Tg/m, right column of Figure 2) into maps of MTZ hydration density (kg of water per square km of MTZ), which are more useful for comparing to IPV eruptions. For this, we express regassing fluxes at subduction zones on a mesh of 10094 nodes distributed with relatively uniform spacing (~225 km at the surface) over a sphere (Figure S2). This results in a mapping of the water flux from the surface into the mantle at a particular time. We assume that water subducts vertically downward into the mantle beneath trench segment midpoints with a constant sinking velocity v_{sink}, which allows us to translate the water flux map to a specific mantle depth. Average upper mantle sinking velocities of 1-4 cm/yr [*van der Meer et al.*, 2018], 1.5-6.0 cm/yr [*Domeier et al.*, 2016], 5-7 cm/yr [*Goes et al.*, 2011], and 10 cm/yr [*Bercovici and Karato*, 2003] have been suggested. Here we employ v_{sink} as an unknown parameter and examine values in the range of 1-9 cm/yr above 660 km depth.

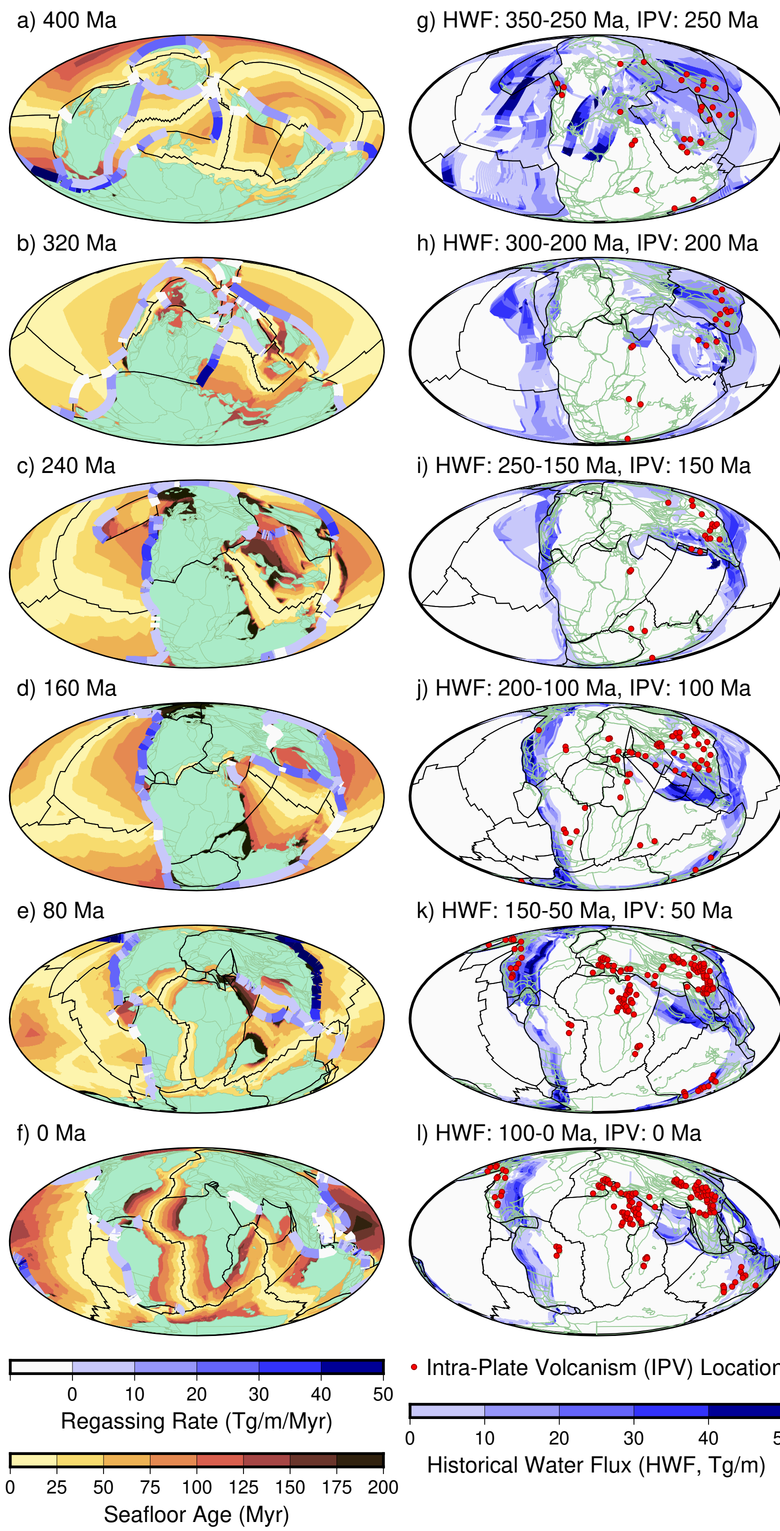

Figure 2. Regassing rates for subduction zone segments (left column) *colored according to the amount of water per unit length of subduction zone segment (per Myr) at (a) 400 Ma, (b) 320 Ma, (c) 240 Ma, (d) 160 Ma, (e) 80 Ma, and (f) 0 Ma (present day). Subduction zone segments that do not contribute to the deep mantle water flux (because they are too warm or subduct too slowly) are displayed as white segments. Also shown for context are reconstructed seafloor ages (colors in oceanic regions, from Karlsen et al. [2019]), plate boundaries (black lines), and continental blocks (green regions).* ***Historical water flux (HWF) and intraplate volcanism (IPV) eruption locations (right column)****, shown at (g) 250 Ma, (h) 200 Ma, (i) 150 Ma, (j) 100 Ma, (k) 50 Ma, and (l) 0 Ma (present-day). Here HWF (colors) represents the mass of water (per unit trench length) that has been injected into the deep mantle by subduction during the previous 100 Myrs (plotted using 1 Myr intervals). Our analysis compares representations of HWF to observed IPV locations, which are shown by red circles (see text for how IPV locations are determined).*

As they encounter the lower mantle, slabs are thought to slow down (e.g., *Butterworth* *et al.* [2014] estimated sinking rates of 1.3 cm/yr in the lower mantle), a process that may already begin in the MTZ. Some slabs appear to penetrate through the MTZ, whereas other slabs stagnate there for a period of time (Figure 1; [*Goes et al.*, 2017]). For scenarios of slab stagnation, we apply a sinking rate of 0 cm/yr at the 660 km discontinuity for a time t_{MTZ}, which we refer to as the MTZ residence time. We note that the effective MTZ residence time may be longer than the time that slabs actually stagnate in the MTZ. This is because any water that is released from a stagnating slab can be stored within wadsleyite and ringwoodite in the MTZ, even after the slab itself has moved deeper into the mantle. Because the duration of slab stagnation is unknown, we employ t_{MTZ} as another unknown parameter and examine plausible scenarios that include t_{MTZ} of 0, 30, and 100 Myr, after which we remove this water from the MTZ. We also consider an "infinite" end member case, named $t_{MTZ}=\infty$, in which all regassed water that reaches the MTZ stays there until the end of the simulation.

Within the upper mantle, water in the slab may migrate or diffuse into surrounding minerals [*Demouchy and Bolfan-Casanova*, 2016], which increases the lateral reach of the subducted water. In addition to diffusion, the location of the water may deviate from the surface location of the trench because slabs dip and deform as they descend, and may drift horizontally if they stagnate [*Goes et al.*, 2017]. To account for the lateral movement of water after subduction as well as uncertainties related to reconstructed subduction zone locations, we distribute water from each subduction zone segment into the *N* closest neighbor mesh points that surround the segment midpoint, with closer points getting more water (Supplementary Text S2). We use *N*=10, which distributes the water within a radius of about 390 km of the segment midpoint (Figure S2) and is consistent with slow diffusion processes [*Demouchy and Bolfan-Casanova*, 2016]. Sensitivity experiments show that increasing *N* has only a modest effect on the water distribution within the MTZ (Supplementary Text S2). Instead, the lateral coverage of water in the MTZ is more closely related to slab stagnation (section 3.2 below). This is because slab stagnation retains water within the MTZ while subduction locations, and thus MTZ injection points, dictate its distribution. The largest control on the lateral extent of MTZ hydration is thus exerted by changing the MTZ residence time t_{MTZ}.

2.2 Location of continental intraplate volcanism

To identify locations of continental intraplate volcanism (IPV), we selected all onshore basalts classified as "Intraplate Volcanism" from the GEOROC (Geochemistry of Rocks of the Oceans and Continents, https://georoc.eu/) database [*Lehnert et al.*, 2000] with assigned eruption ages within the most recent 250 Myr. The choice of 250 Myr allows time for the tectonic reconstruction to populate the MTZ with water following the start of the tectonic reconstruction at 410 Ma. We did not include sites classified as ocean islands, as a majority of those sites are likely related to mantle plumes, and thus a deep mantle source below the MTZ. Furthermore, oceanic intraplate volcanism is continually erased by subduction, which makes the oceanic IPV record uneven and incomplete. Although some of the continental IPV points in the dataset are likely also related to plumes, we did not attempt to remove such points because it is difficult to distinguish plume-associated IPV from other IPV. Thus, we used the database "as-is" (downloaded on November 16, 2021) to avoid selection bias. Importantly, the database shows only the present-day location of IPV, but due to plate motions most of these sites were in a different location at the time of their emplacement. Therefore, we computed the original position of each IPV point according to the same plate reconstruction model used to estimate the water flux to the mantle [*Matthews et al.*, 2016; *Torsvik et al.*, 2019], yielding maps of IPV locations for past times (Figure 2, right column). For comparison to MTZ hydration, we also filtered the data to exclude duplicate points and merged clustered points to mitigate oversampling (Supplementary Text S3; Figure S3).

2.3 Occurrence of IPV above wet or dry mantle

Having developed models for MTZ hydration and IPV eruption as a function of time and space (Figure 2); we now seek to determine if there exists any meaningful correlation between them. We might anticipate a delay period (t_{IPV}) between the charging of the MTZ with water and the eruption of IPV at the surface, associated with the ascent rate of hydrous upwellings from the MTZ and the time for melt to penetrate the lithosphere. Previous studies suggest IPV delay periods of ~12 Myr [*Yang and Faccenda*, 2020], tens of Myr [*Motoki and Ballmer*, 2015], and 10-30 Myr [*Long et al.*, 2019]. Therefore, we compare IPV maps (e.g., Fig. 2, right column) with MTZ hydration maps that are older by t_{IPV} delay periods of 0, 10, 20, 30, and 50 Myr.

We interpolate our MTZ hydration models (section 2.1) to determine the concentration of water in the MTZ beneath each IPV point. To identify regions of the MTZ where subducted water may have accumulated, we choose a threshold of $0.5 \cdot 10^9$ kg/km^2 to define the 'wet mantle transition zone', while values below this cutoff are designated as 'dry'. This threshold, which equates to a layer of water 0.5 m thick distributed within the 250 km thickness of the MTZ, lies just above the minimum non-zero MTZ water content in our maps (e.g., Figure 3). It is ~20 times smaller than 0.001 wt % water, which is the cutoff used by *Zhang et al.* [2022] to define the "dry" MTZ. We use a more generous definition of the "wet" MTZ because we want to include all regions of the MTZ that may have retained any water from slabs. We note that even small amounts of water can cause reduced viscosity and melting of mantle rocks [*Drewitt et al.*, 2022; *Hirschmann*, 2006; *Luth*, 2003; *Wright*, 2006]. We use a wet/dry distinction, rather than using water concentrations directly, because we only consider the presence of IPV; we do not consider eruption volumes in our analysis. Furthermore, we do not know how much water is needed to promote IPV, and other factors that may affect the formation of IPV are poorly constrained. Therefore, we do not attach extra importance to IPV occurrences above higher MTZ water concentrations.

For a quantitative measure of the degree of correlation between IPV and wet MTZ, we determined the percentage of volcanic eruptions located vertically above "wet" MTZ. We compared IPV and wet MTZ in this way for each 1 Myr time increment in the past, and averaged over the period 250-0 Ma.

3 Distribution of water in the mantle transition zone and comparison to IPV

We compare predictive maps of MTZ water content with the changing locations of IPV through the past 250 Myr. We start by examining a reference scenario based on specific choices for t_{MTZ}, v_{sink}, and t_{IPV}. By adjusting these parameters, we develop alternative models for the timing of MTZ hydration, which we test against observed IPV patterns for t_{MTZ}, v_{sink}, and t_{IPV}.

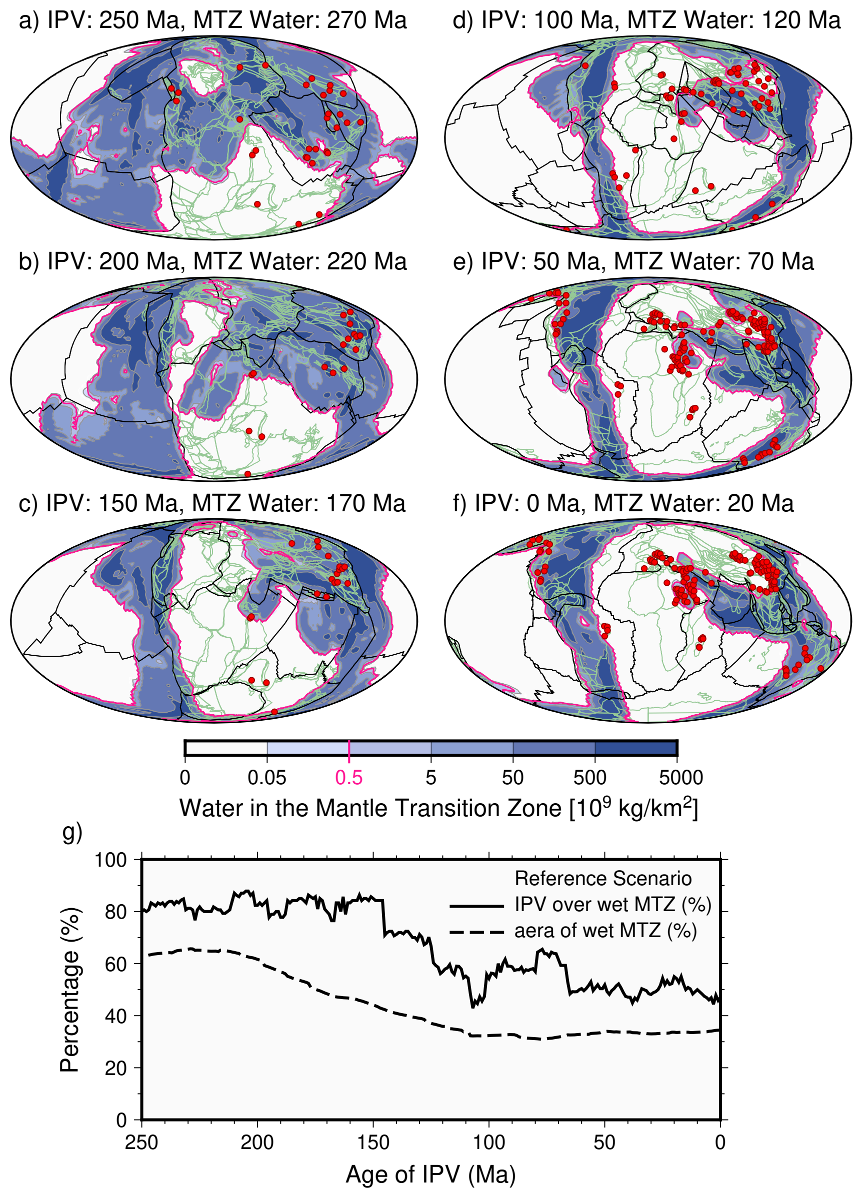

Figure 3. Comparison of IPV locations to the MTZ water distribution, for the reference scenario. *(a-f) Predictions of the water distribution in the mantle transition zone (colors) and locations of active intraplate volcanism (IPV, red points), for times between the present-day (a) and 250 Ma (f), with reconstructed coastlines (green lines) and plate boundaries (black lines). The reference scenario shown here assumes that water has a residence time of t_{MTZ} = 100 Myr in the MTZ, a slab sinking velocity of v_{sink} = 3 cm/yr, and a t_{IPV} = 20 Myr delay before IPV eruption. (g) Percentage of IPV locations that lie above wet MTZ (defined as $\geq 0.5 \cdot 10^9$ kg/km^2, pink contour in a-f) for this reference scenario (solid line). Shown for comparison is the fraction of the reference grid area that is covered by hydrated (rather than dry) MTZ regions (dashed line).*

3.1 The reference scenario

For our reference scenario, we apply a sinking rate of v_{sink} = 3 cm/yr, an MTZ water residence time of t_{MTZ} = 100 Myr, and an IPV delay period of t_{IPV} = 20 Myr. This model predicts that at 20 Ma (Figure 3f) the hydrated portion of the MTZ extended across regions of the mantle transition zone beneath present-day South and North America, the western Pacific and eastern Asia, and beneath India and some of the Middle East. This hydrated MTZ reflects patterns of Cenozoic subduction, which is expected given that slabs sinking at 3 cm/yr will reach the MTZ after only 15-20 Myr. Because subduction migrates slowly, this same geographical pattern has persisted since the Cretaceous (Figures 3d to 3f), with about one third of the MTZ being hydrated since 120 Ma (Figure 3g). Before the Cretaceous, the hydrated part of the MTZ covered a larger area, exceeding 60% of the MTZ area during 200-250 Ma (Figure 3g). However, much of the wet MTZ was only weakly hydrated during the Jurassic and earlier (Figures 3a and 3b), reflecting slower regassing rates prior to a peak at ~130 Ma [*Karlsen et al.*, 2019]. The area of the wet

MTZ was greater during these earlier periods because of faster trench migration rates in the tectonic reconstruction prior to ~250 Ma, perhaps resulting from ocean basin closure during supercontinent assembly [*Young et al.*, 2019].

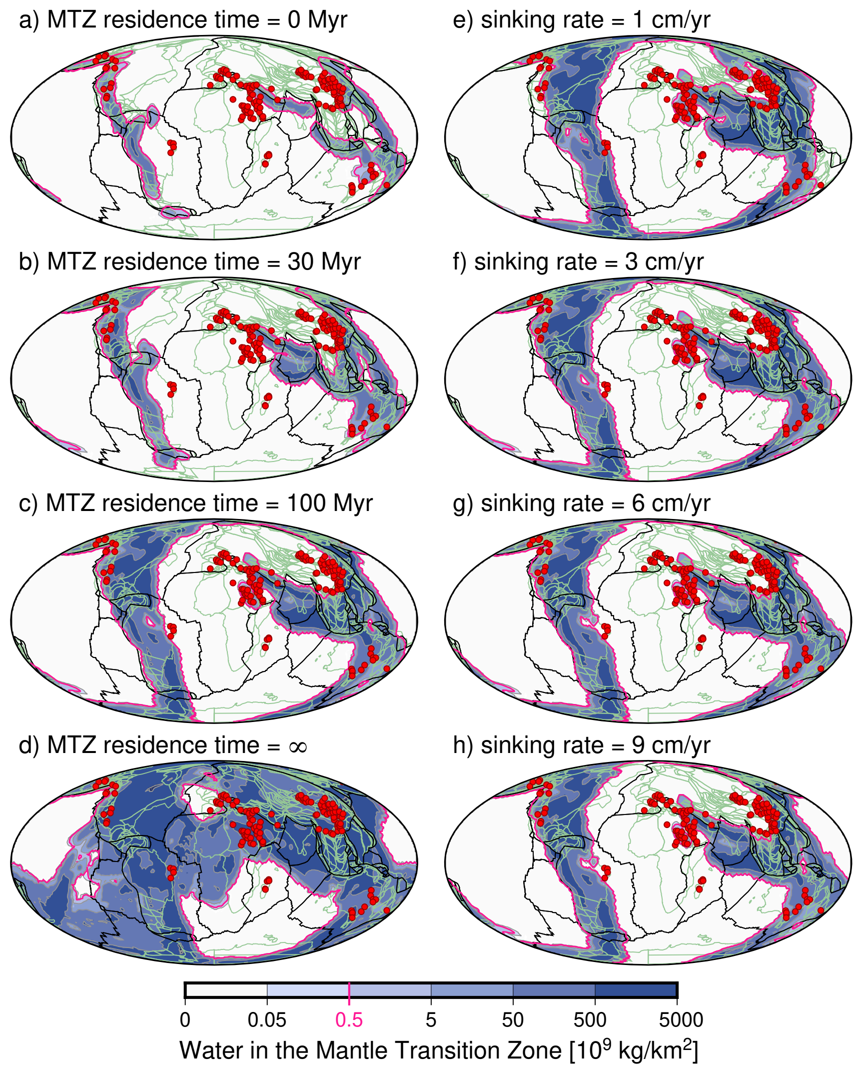

Figure 4. Effect of varying MTZ water residence time and slab sinking rates. Predictions of the water distribution in the mantle transition zone (MTZ) at 20 Ma for (a-d) varying MTZ residence time t_{MTZ} (assuming v_{sink} = 3 cm/yr and t_{IPV} = 20 Myr) and (e-h) varying slab sinking rate v_{sink} (assuming t_{MTZ} = 100 Myr and t_{IPV} = 20 Myr). Shown for all plots are continental outlines (green lines), plate boundaries (black lines) and active intraplate volcanism (IPV) locations (red dots) at 0 Ma. The pink contour outlines the wet MTZ (defined as $\geq 0.5 \cdot 10^9$ kg/km^2).

We compare the 132 IPV samples for the present day (0 Ma) to the MTZ at 20 Ma, accounting for the t_{IPV} = 20 Myr delay time before eruption (Figure 3f). We find that 47% of the 132 IPV samples overlie a wet MTZ (Figure 3g). Many of these "wet" IPV locations lie in eastern Asia and western North America (Figure 3f). Several points are located above MTZ that is only slightly hydrated, and some "dry" IPV locations are positioned near the edge of hydrated MTZ. Allowing for faster lateral spreading of hydration, or permitting greater MTZ water residence time, would likely result in more IPV overlaying wet MTZ. This correlation of IPV with the edges of the wet MTZ persists for IPV at 50 Ma (compared to the MTZ at 70 Ma, Figure 3e) and earlier in the Cretaceous, during which ~40-50% of IPV is underlain by wet MTZ (Figure 3g). The correspondence between IPV and wet MTZ is higher at 250 and 200 Ma (Figures 3a and 3b), with more than ~80% of IPV underlain by MTZ that was wet 20 Myr prior (Figure 3g). This higher percentage likely results from a more geographically expansive wet MTZ before the Cretaceous. Across 0 to 250 Ma, an average of 66.6% of the IPV locations reconstruct above MTZ that was wet 20 Myr before eruption.

3.2 MTZ water residence time

By varying the MTZ residence time t_{MTZ}, we show that the volume of water in the MTZ increases with increased residence time, as expected (Figure 4a-d). At 20 Ma (the time that is compared to present-day IPV for t_{IPV} = 20 Myr), wet conditions extend across only ~13% of the MTZ area for t_{MTZ} = 0 Myr (water sinks through the MTZ in less than 9 Myr at 3 cm/yr), but across ~74% if the MTZ if the residence time is unlimited (t_{MTZ}=∞) (Figure 5a). This trend is also evident for past times (e.g., at 100 and 200 Ma, Figure S4), where wet conditions tend to quickly "fill up" the MTZ for longer MTZ residence times. Because of this greater area-coverage of wet conditions, we find that more IPV locations lie above hydrated MTZ for longer residence times (Figure 5a). As for the reference scenario (Figure 3a), the fraction of IPV underlain by wet MTZ is nearly always larger than the area fraction of the wet MTZ (Figure 5a). This means that IPV locations preferentially occur above the wet MTZ.

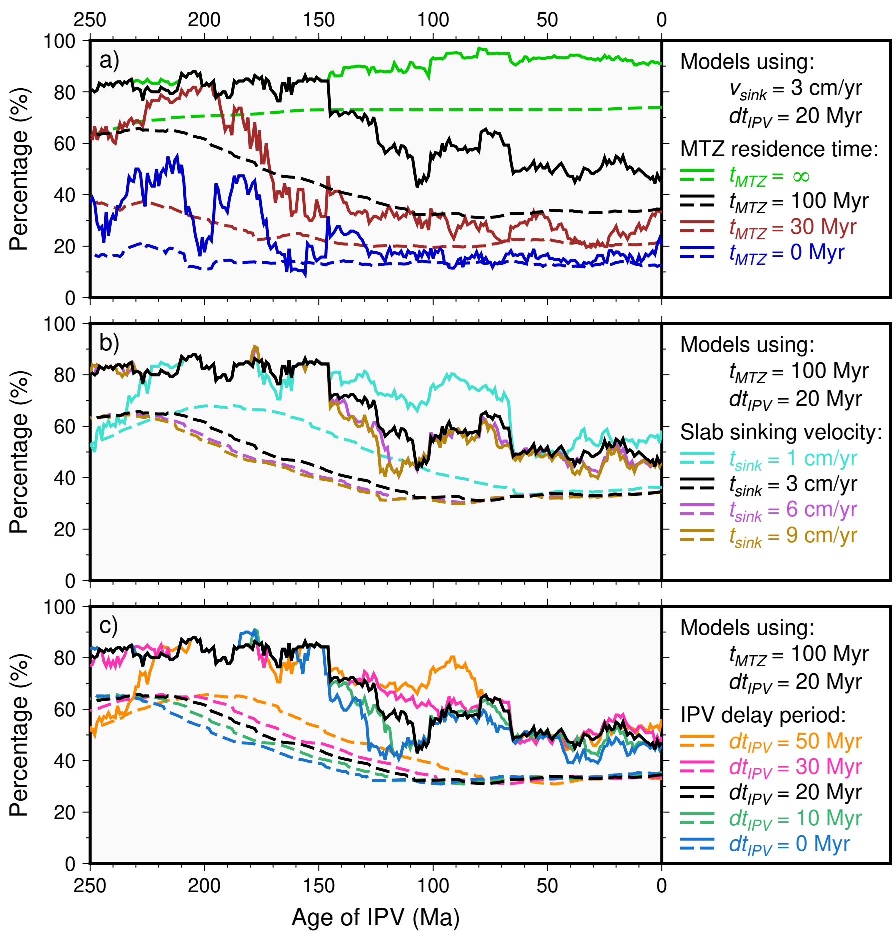

Figure 5. Comparisons of intraplate volcanism (IPV) locations with the hydrated mantle transition zone (MTZ) for different scenarios. *Shown is the fraction of IPV locations positioned above wet MTZ (solid lines) and the representative fraction of grid area covered by wet (rather than dry) MTZ regions (dashed lines). (a) Varying MTZ residence times (t_{MTZ}) for scenarios with v_{sink} = 3 cm/yr and t_{IPV} = 20 Myr. (b) Varying slab sinking rates (v_{sink}) for scenarios with t_{MTZ} =100 Myr and t_{IPV} = 20 Myr. (c) Varying IPV delay periods (t_{IPV}) for scenarios with t_{MTZ} =100 Myr and v_{sink} = 3 cm/yr. The black lines reproduce the lines in Figure 3g, i.e., the reference scenario.*

3.3 Slab sinking rate

The slab sinking rate v_{sink} determines the time it takes for subducted water to reach the MTZ, and a slower sinking rate extends the time that water spends within MTZ. However, varying the slab sinking rate between 1 and 9 cm/yr does not significantly change the predicted water distribution within the MTZ (Figure 4e-h), although more water is present within the MTZ for slower sinking rates (at 20 Ma, 36.3% of the MTZ is wet for v_{sink} = 1 cm/yr compared to 34.4% for v_{sink} = 9 cm/yr). Across the past 250 Myr (Figure 5b), a slow 1 cm/yr slab sinking rate results in a slightly better average match between IPV and wet MTZ than for faster sinking rates.

3.4 IPV delay period

Because the wet MTZ changes only gradually with time (e.g., Figure 3), the IPV delay period t_{IPV}, even one as long as 30 or 50 Myr, does not significantly affect the correlation between hydrated regions of the MTZ and IPV eruptions (Figure 5c). This parameter (t_{IPV}) also does not affect the area of wet MTZ (dashed lines, Figure 5c), but effectively shifts it to younger ages (rightward in Figure 5c) because IPV eruption locations are compared to the MTZ at the (older) time before the delay.

4 Statistical significance of correlations

We use a statistical approach to determine whether the observed correlations between IPV locations and the hydrated regions in the MTZ can be considered significant. Specifically, we seek to test the null-hypothesis that the observed correlation can be explained as a chance occurrence. To achieve this, we compute the observed fit against a set of randomly perturbed trials and conduct a one-tailed test. This allows us to determine the *p*-value, which is a measure of the likelihood of obtaining a correlation as large or larger than the observed value by random chance, i.e., the null-hypothesis. A small *p*-value (typically $p \leq 0.05$) suggests that the null-hypothesis is unlikely, and can be rejected.

To develop a set of random comparisons from which to derive an empirical distribution, we randomly re-oriented (see Supplementary Text S4) the simulated MTZ water grid (as constructed for a given set of model parameters). To obtain a statistically significant sample, we re-oriented each MTZ water grid 10^4 times, applying the same re-orientation for each time-step (within 0-250 Ma) of a given model. We then determine the fraction of IPV locations (which remain unperturbed) occurring above wet MTZ for each randomly re-oriented MTZ grid (see examples in Figure S5), and find the average over 250 million years, as before. Applying this procedure to the 10^4 different random rotations, we construct a distribution of wet IPV fractions for these "randomized wet MTZ scenarios" (Figure 6). The *p*-value is given as the fraction of this empirical distribution with a correlation between IPV and wet MTZ that is in excess of the observed value. If less than 5% of the random re-orientations yield a higher wet IPV fraction ($p < 0.05$ in Figure 6), then we can conclude that the observed correlation between IPV locations and the wet MTZ is not random. Note that the p-value that we obtain using this method is independent of the number of volcanism samples and is valid even if IPV sampling is incomplete [*Conrad et al.*, 2011]. This approach was applied to all scenarios of this study to determine which correlations may be statistically significant.

For the reference scenario, 66.6% of IPV locations since 250 Ma are underlain by wet MTZ (Figure 5a and Section 3.1). Of the 10^4 re-oriented MTZ water grids, only 3.9% produced correlations greater than 66.6% (Figure 6, top). This corresponds to a p-value of 0.039, which satisfies $p < 0.05$ and means that we can reject the null hypothesis (that the observed correlation between IPV and wet MTZ is a chance occurrence) at the 95% confidence level. Applying the same procedure to the other models for the wet MTZ, in which we vary t_{MTZ}, v_{sink}, and t_{IPV}, (Figure 6), we find that several other models exhibit correlations that are statistically significant at the 95% confidence level ($p \leq 0.05$). In particular, we find that changes to the reference scenario with t_{MTZ} of 30 to 100 Myr, v_{sink} of 3 cm/yr or more, and t_{IPV} between 10 and 30 Myr, can all produce correlations that are statistically significant at the 95% confidence level (Figure 6). These statistical tests suggest that there could be a meaningful link between the occurrence of IPV and hydrated regions of the MTZ, at least for the reference scenario and a range of models that are similar to it.

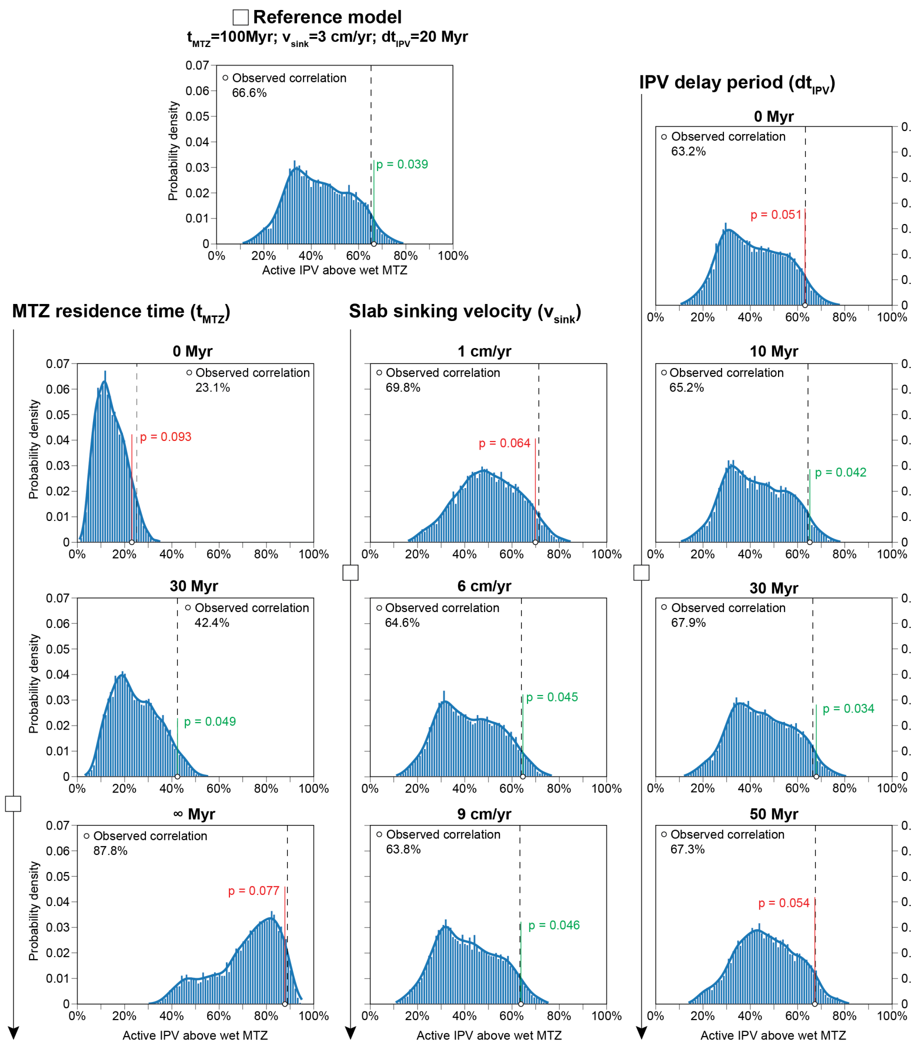

Figure 6. Distribution of correlations between IPV locations and randomly-oriented wet MTZ for the various models of this study. *The scenarios examined include the reference scenario (top left, marked with □), and variations to it involving the MTZ residence time (t_{MTZ}, left column), the slab sinking rate (v_{sink}, middle) and the IPV delay period (t_{IPV}, right). Here the observed correlation between IPV locations and wet MTZ is drawn with a black dashed line (observed value given in black). The percentage of the distribution with a correlation larger than observed is given by the p value, with $p < 0.05$ (shown by green labels) indicating that the observed correlation between IPV and wet MTZ is unlikely to result from random chance. In the remaining cases ($p > 0.05$, red labels) the null hypothesis cannot be rejected at the 95% confidence level.*

5 Discussion

We have estimated the rates and volumes of water transport into the deep mantle from modeled subduction fluxes based on plate tectonic reconstructions spanning 400 Myr. From these, we quantified the spatial heterogeneity of water in the MTZ. We find a statistically significant correlation between predicted hydrous regions of the MTZ and the locations of intraplate volcanism. Models with a statistical significance above the 95% confidence level display a match with continental intraplate volcanism between 42-68% (Figure 6), suggesting that over the past 250 Myr a large fraction of IPV has occurred above wet regions of the mantle.

We considered multiple models as defined by choices for several different variables that control the distribution of subducted water in the MTZ. We find that the alignment of IPV locations with the wet MTZ in our models depends significantly on the MTZ water residence time (t_{MTZ}), while the slab sinking rate and IPV delay time are less important. We find a p-value ≤ 0.05 for models with t_{MTZ} between 30 and 100 Myr (Figure 6). Outside of this range, shorter MTZ residence times (e.g., 0 Myr) do not generate enough MTZ hydration to explain IPV at a level that is statistically significant, while longer MTZ residence times (e.g., ∞ case) add water to so much of the MTZ that even randomly-placed IPV locations are likely to sit above wet MTZ. This suggests that the temporary stagnation of slabs at the 660 km discontinuity, for periods of ~30 Myr or more, is crucial for MTZ hydration, and this hydration provides opportunities for generating IPV.

The fact that different choices of slab sinking rate and IPV delay time do not significantly affect correlations between IPV and wet MTZ, except for their most extreme values, suggests that these parameters are not significantly important to their linkage. We did observe a poor correlation (and less statistical significance) for the slowest sinking rate of 1 cm/yr (Figure 6); this indicates that a slow upper mantle sinking rate is not by itself sufficient to produce patterns of wet MTZ that are sufficiently correlated to IPV. Instead, it seems that stalling in the MTZ for ~30-100 Myr is necessary. Concerning the IPV delay period, the most statistically-significant result is for a delay period of 30 Myr (Figure 6), which supports the expectation of a nonzero IPV delay period because hydrous melt must be created, ascend to the asthenosphere, and travel through the lithosphere, to cause volcanic eruptions. However, the timing of these processes is still poorly understood and more research is needed to constrain the process of IPV generation by hydrous melt.

5.1 Implications of a correlation between IPV and wet MTZ

Establishing that IPV patterns correlate with hydrous MTZ regions supports the widely recognized hypothesis that water is transported to the MTZ by subducting slabs [*Bodnar et al.*, 2013; *Kelbert et al.*, 2009; *Magni et al.*, 2014; *Thompson*, 1992; *van Keken et al.*, 2011], and consequently generates spatial and temporal mantle heterogeneity [*Peslier et al.*, 2017]. This also suggests that tectonic reconstruction models are a valuable tool for exploring and estimating this heterogeneity. Generally, the MTZ water distribution over the period investigated (0-250 Ma) reflects continuous hydration of particular regions with a long history of subduction. Many of these regions are overlain by IPV (e.g., Figure 3). Such a link between a locally hydrated mantle transition zone and volcanism far from plate boundaries has been suggested by previous studies that mainly focused on a regional scale, for example the Cenozoic IPV in Northeast China

[*Kuritani et al.*, 2011; *Yang and Faccenda*, 2020]. Our study confirms this link, but globally and in a statistical sense, for IPV that erupted during the past 250 Myr.

Upwelling from hydrated parts of the MTZ, and the subsequent generation of melting and IPV eruption, may be a complicated process involving multiple geodynamic processes. For example, hydrous upwelling itself may require multiple subduction events to first saturate the MTZ and then to trigger upwelling flow of hydrated mantle [*Kuritani et al.*, 2011; *Yang and Faccenda*, 2020]. Therefore, although the presence of water in the MTZ is likely to promote IPV, it must do so in conjunction with mantle processes that operate on MTZ heterogeneity over time, including several that draw the mantle above stagnant slabs upward [*Kameyama and Nishioka*, 2012; *Kelbert et al.*, 2009; *Long et al.*, 2019]. Once hydrated rocks are in the asthenosphere, other processes such as shear-driven upwelling [e.g., *Ballmer et al.*, 2015; *Conrad et al.*, 2011], lithospheric deformation [e.g., *Valentine and Hirano*, 2010], and small-scale convection [e.g., *Ballmer et al.*, 2010; *King and Ritsema*, 2000] may be important to produce localized melting and eruption to the surface. Although we do not directly include such secondary processes within our models, we indirectly account for them when using large values of t_{MTZ} and t_{IPV}, for which we obtain the largest correlations between IPV and wet MTZ.

Among the parameters we consider, the strongest control appears to be exerted by the MTZ water residence time (t_{MTZ}), which implies that slab stagnation is important to MTZ hydration. The extra time that stagnating slabs spend in the MTZ may provide opportunities for incorporation of subducted water into the hydrous reservoirs of the MTZ [e.g., *Kuritani et al.*, 2011], which we have now associated with IPV at the surface. Storage of this water in the MTZ, even if temporary, removes water from the Earth's surface reservoirs, decreasing sea level [e.g., *Karlsen et al.*, 2019]. The presence of this water within the MTZ minerals of ringwoodite and wadsleyite may also be important for reducing MTZ viscosity toward observed values [*Fei et al.*, 2017], affecting global mantle flow patterns [e.g., *Karato*, 2011] and Earth's long-term thermal evolution [e.g., *Crowley et al.*, 2011]. Water loss from the MTZ may occur as mantle flow brings hydrated minerals across the upper [*Andrault and Bolfan-Casanova*, 2022] or lower [*Schmandt et al.*, 2014] boundaries of the MTZ. The addition of water to the assemblage of nominally anhydrous minerals in these regions results in melting, and the melt likely percolates upward [*Ohtani et al.*, 2018]. Melt that forms above the MTZ eventually reaches the asthenosphere, and can be erupted by IPV [*Andrault and Bolfan-Casanova*, 2022], as discussed above. Melt forming below the MTZ may also percolate upward, re-hydrating the MTZ [*Schmandt et al.*, 2014], but some water likely remains stored within lower mantle bridgmanite, and continues downward [*Walter*, 2021]. Our results suggest that these processes overall lead to an average longevity of water in the MTZ of order 30-100 Myr, with much uncertainty.

It is notable that we observe better agreement between IPV locations and the hydrated MTZ for earlier times (~125-250 Ma). This is the opposite of what we might expect given that the uncertainties on both the plate reconstruction and the IPV database generally increase with time. However, large regassing rates early in the tectonic reconstruction (before 320 Ma, Figure S1e) and rapid trench migration [*Young et al.*, 2019] may have hydrated significant parts of the MTZ during the period ~400-200 Ma. The storage of this water in the MTZ for periods of up to 100 Myr (large MTZ residence times) may have induced IPV across a wide region during the first part of our analysis (~250-150 Ma). Alternatively, the decreasing number of IPV samples for older times (Figure S3c) may indicate sampling bias. If this bias involves preferential sampling of eruptions that are larger in magnitude (greater eruptive volume), then it is possible that such larger-scale IPV events are more likely to be related to melting of hydrous upper mantle, which should produce greater melt volumes. By contrast, the database of recent IPV may over-represent small-scale events that are less likely to be related to wet MTZ.

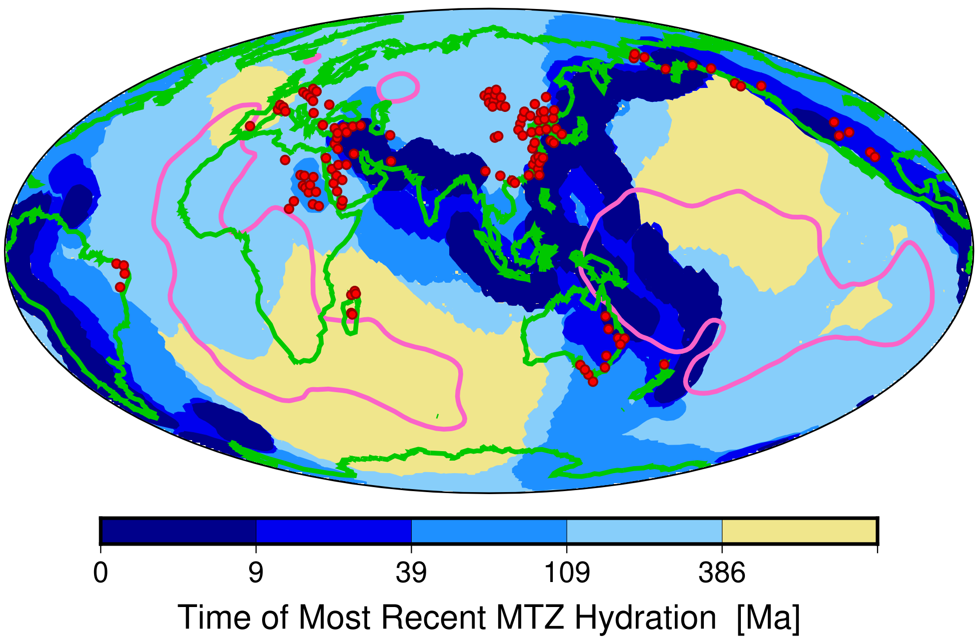

Figure 7. Map of the time of the most recent MTZ hydration *(colors), as compared to current IPV volcanism (red dots), continental locations (green lines), and LLSVP locations at the base of the mantle (pink lines). Here we assume a slab sinking rate of 3 cm/yr, and plot colors based on the ages of interaction of these slabs with the MTZ model for the four different choices of* t_{MTZ} *that we examined. We note that three major areas of the MTZ (regions with yellow colors, near western Europe, southern Africa and the western Pacific) have not interacted with hydrated slabs in the past 400 Myr.*

5.2 Dry regions of the mantle transition zone

The water mapped in this study is transported to the MTZ through subduction. Therefore, areas that have remained far from subduction zones throughout the considered period should be relatively dry (Figure 7), unless ancient water has remained stable for longer periods (> 400 Myr) or water has been transported into these regions by other means. This suggests that the MTZ beneath the Indian Ocean, Southeast Africa, the South Atlantic Ocean, large parts of the North Pacific Ocean, and a modest area below western Europe have remained dry for the past 400 Myr, and should be dry today. We note that there is relatively little IPV above the "dry" areas, although many of these regions are covered by oceanic lithosphere, where we have not considered IPV. These "dry" areas away from subduction zones roughly correspond to areas of persistent and stable broad-scale upwelling in the mantle [*Conrad et al.*, 2013], which represents a return-flow from subduction downwelling occurring around these areas [*Shephard et al.*, 2017]. Intraplate volcanism has been identified within these regions away from subduction, but it has been mostly associated with deep mantle plumes (e.g., Hawaii). Plume-induced intraplate volcanism has been associated with the edges of the Large Low Shear Velocity Provinces (LLSVPs) at the base of the mantle, which form away from subduction zones [*Torsvik et al.*, 2016]. Some of the IPV identified within the "dry" areas of the MTZ (Figure 7) may thus be associated with plumes rising from the deep mantle.

Because the presence of water tends to reduce viscosity of the MTZ [*Fei et al.*, 2017], these dry regions should have a larger viscosity than the wetter areas that surround them. This increased viscosity may be partially offset by decreased viscosity associated with mantle upwelling and increased temperatures associated with these regions away from subduction zones [*Conrad et al.*, 2013]. However, if these dry regions of the MTZ are indeed stiffer than their surroundings, then mantle deformation should preferentially occur in the wetter areas, affecting upper mantle flow patterns [*Ramirez et al.*, 2023]. Indeed, subduction-related deformation has tended to occur away from these potentially dry areas above the LLSVPs [*Shephard et al.*, 2017], preventing hydration of these areas of the MTZ (Figure 7) and perhaps stabilizing large-scale mantle flow patterns [*Conrad et al.*, 2013]. A dry MTZ may also exert an important influence on rates of glacial isostatic adjustment (GIA), which includes the solid Earth's viscous response to episodes of deglaciation. Indeed, one of the dry regions in our models is predicted to extend beneath East Antarctica (Figure 7). Here, elevated upper mantle viscosities have been shown to slow rates of uplift in response to past (and future) deglaciation there, with important implications for sea level change [*Gomez et al.*, 2024].

5.3 Limitations

Uncertainties in the generated MTZ water grids are partly linked to and controlled by the underlying plate tectonic model [*Karlsen et al.*, 2021; *Karlsen et al.*, 2020; *Matthews et al.*, 2016; *Torsvik et al.*, 2019], which becomes increasingly poorly constrained for older time periods. We assume vertical subduction, which has been suggested to be reasonable for mapping subducted slabs [*Domeier et al.*, 2016], but does not account for lateral deflections or slab stagnations that may affect the MTZ water content. Thus, we have had to introduce additional parameterizations, such as the threshold for wet MTZ and the number of nearest neighbors used to spread the water laterally. These choices are poorly constrained and affect the MTZ water distribution and its link to IPV. We argue that the statistical approach used here (section 4) allows us to overcome this uncertainty by looking for overall correlations, even weak ones, based on "best guess" choices for some of these unknown parameters. Of course, this means that our predictive maps of MTZ hydration include a significant degree of uncertainty.

We have shown that one of the most important parameters is the MTZ residence time, which is related to slab stagnation. However, not all slabs behave the same way; some may stagnate for different amounts of time in the MTZ while other slabs may subduct directly through it. Therefore, our assumption of using one constant value of MTZ residence time per model is a significant simplification. A more detailed mapping of wet and dry regions in the mantle transition zone (Figure 7) could be constructed by considering these different behaviors for each slab. It could be possible to infer slab topology from tomographic models for recent times, but would unfortunately be difficult, if not impossible, to do so for past times. However, if we assume that there is indeed a link between wet MTZ and the occurrence of IPV, one could use the location and ages of IPV to speculate on the temporal and spatial variations of the MTZ hydration state back in time.

Our hypothesis testing using IPV locations may be limited by the geochemical dataset that we used. In particular, we are heavily dependent on the classifications of volcanism within the GEOROC database [*Lehnert et al.*, 2000]; we only considered intraplate volcanism with basaltic compositions. We did not attempt to remove plume-related events, except that we only considered continental locations. Thus, there are an unknown number of "IPV" samples in our dataset that have a plume source, e.g., the Afar plume below the African rift. The ability to remove these points is hindered by limited knowledge of past plume events; known hotspot volcanism was therefore not filtered out to preserve consistency.

One of the greatest uncertainties of the statistical test is our choice of $0.5 \cdot 10^9$ kg/km^2 for the threshold between wet and dry MTZ. A low threshold is reasonable as even a tiny amount of water can generate melt production if the mantle conditions are close to the solidus, although more water is needed to produce melting in colder regions [*Karato et al.*, 2020; *Katz et al.*, 2003] and buoyant hydrous upwelling requires significant hydration [*Yang and Faccenda*, 2020]. However, other mechanisms that require less water may help to link the wet MTZ to IPV. We note that the specific choice of a threshold may not be too important, because the area covered by water values between 0.05 and $5 \cdot 10^9$ kg/km^2 is rather small compared to the overall "wet" area (Figures 3 and 4). However, choosing a larger value for the threshold may impact the match percentages between the wet MTZ and IPV locations, and the statistical significance of these matches. Alternatively, it could be useful to investigate correlations between the degree of MTZ hydration and the volumes of IPV. However, the IPV database that we are using does not include constraints on volumes of IPV, and such constraints are difficult to obtain anyway. Overall, an improved understanding of the mechanism behind non-hotspot IPV is needed to choose a more appropriate value for this threshold.

6 Conclusions

Our study suggests that the mantle transition zone (MTZ, 410-660 km) is likely to be heterogeneously hydrated, with wetter regions beneath areas with a long history of subduction, and regions away from subduction remaining dry (Figure 7). To show this, we created maps of the spatial and temporal heterogeneity of water storage in the mantle transition zone (e.g., Figure 3), based on tectonic reconstructions for the last 400 Ma and the assumption that subduction transports water downward into the MTZ. Using these maps, we discovered a positive correlation between wet regions of the MTZ and locations of intraplate volcanism (IPV) at the surface (Figure 5), and we demonstrated that this correlation is statistically significant (Figure 6). In particular, we showed that water must reside in the MTZ for long periods (timescales of 30 to 100 Myr) in order for the hydrous regions of the MTZ to be positively correlated with IPV in a statistically significant way (>95% confidence that the association is not random). This is because slab stagnation at the MTZ allows for slab dehydration and water accumulation in the surrounding MTZ rocks. We also found that a time delay of 10 to 30 Myr between MTZ hydration and IPV eruption tends to produce better correlations. This long MTZ residence time and long IPV delay time suggest that significant time and perhaps multiple subduction events are required to hydrate the MTZ, mobilize the hydrated mantle to generate melt, and transport this melt upwards for eruption at the surface.

The MTZ water distribution, as characterized by our predictive maps (Figures 3 and 4) is mostly dictated by tectonic patterns of subduction at the surface, including the plate convergence rate, trench migration rate, and subducting plate age for subduction zones around the world [*Karlsen et al.*, 2019]. We find that the area fraction of wet MTZ was likely greater in the past

(>150 Ma), because of a more extensive subduction network that migrated more quickly [*Young et al.*, 2019]. The extent of hydration also depends critically on the residence time of water in the MTZ, as controlled by slab stagnation [*Komabayashi and Omori*, 2006; *Kuritani et al.*, 2011] and possible MTZ rehydration [*Schmandt et al.*, 2014] as water is released from dehydrating lower mantle slabs [*Walter*, 2021]. Also important are processes that generate upwelling and upwards water transport from the hydrous regions of the MTZ [*Kuritani et al.*, 2019; *Wang et al.*, 2015; *Yang and Faccenda*, 2020], leading to melting beneath the lithosphere [*Long et al.*, 2019; *Motoki and Ballmer*, 2015] and eruption at the surface.

Beyond the important implications for IPV that we have detailed here, a heterogeneously hydrated MTZ should also be viscously heterogeneous [*Fei et al.*, 2017]. This is important because MTZ viscosity controls rates of upper mantle flow [*Ramirez et al.*, 2023], planetary thermal evolution [*Crowley et al.*, 2011], and even recent deglaciation-induced solid earth uplift [*Gomez et al.*, 2024]. Thus, new comparisons between geophysical, geologic, and tectonic constraints on the hydration state of the MTZ, exemplified by our study, can help us to understand a variety of important geodynamic processes.

Open Research. The intraplate volcanism database is taken from the GEOROC (Geochemistry of Rocks of the Oceans and Continents, https://georoc.eu/) database, with data available from *Lehnert et al.* [2000]. Mapping of the hydrous regions of the mantle transition zone utilizes the GPlates software [*Müller et al.*, 2018], which can be accesses at https://www.gplates.org, and data from the global plate tectonic model of *Matthews et al.* [2016], corrections for the Pacific from *Torsvik et al.* [2019], and seafloor ages from *Karlsen et al.* [2021].

Acknowledgements. This work was partly supported by the Research Council of Norway via project 288449 (MAGPIE project) and via its Centres of Excellence scheme, project numbers 223272 (CEED) and 332523 (PHAB). We thank Krister Karlsen for valuable assistance with the regassing model, and Stephane Rondenay and Tobias Rolf for reviewing an early version of this manuscript.

References

Aivazpourporgou, S., S. Thiel, P. C. Hayman, L. N. Moresi, and G. Heinson (2015), Decompression melting driving intraplate volcanism in Australia: Evidence from magnetotelluric sounding, *Geophysical Research Letters*, *42*(2), 2014GL060088, doi:10.1002/2014GL060088.

Andrault, D., and N. Bolfan-Casanova (2022), Mantle rain toward the Earth's surface: A model for the internal cycle of water, *Physics of the Earth and Planetary Interiors*, *322*, 106815, doi:https://doi.org/10.1016/j.pepi.2021.106815.

Ballmer, M. D., C. P. Conrad, E. I. Smith, and R. Johnsen (2015), Intraplate volcanism at the edges of the Colorado Plateau sustained by a combination of triggered edge-driven convection and shear-driven upwelling, *Geochemistry, Geophysics, Geosystems*, *16*(2), 366-379, doi:10.1002/2014GC005641.

Ballmer, M. D., G. Ito, J. van Hunen, and P. J. Tackley (2010), Small-scale sublithospheric convection reconciles geochemistry and geochronology of 'Superplume' volcanism in the western and south Pacific, *Earth and Planetary Science Letters*, *290*(1–2), 224-232, doi:http://dx.doi.org/10.1016/j.epsl.2009.12.025.

Bercovici, D., and S.-i. Karato (2003), Whole-mantle convection and the transition-zone water filter, *Nature*, *425*(6953), 39-44, doi:10.1038/nature01918.

Bodnar, R. J., T. Azbej, S. P. Becker, C. Cannatelli, A. Fall, and M. J. Severs (2013), Whole Earth geohydrologic cycle, from the clouds to the core: The distribution of water in the dynamic Earth system, *Geological Society of America Special Papers*, *500*, 431-461, doi:10.1130/2013.2500(13).

Butterworth, N. P., A. S. Talsma, R. D. Müller, M. Seton, H. P. Bunge, B. S. A. Schuberth, G. E. Shephard, and C. Heine (2014), Geological, tomographic, kinematic and geodynamic constraints on the dynamics of sinking slabs, *Journal of Geodynamics*, *73*, 1-13, doi:https://doi.org/10.1016/j.jog.2013.10.006.

Chang, S.-J., and A. M. G. Ferreira (2019), Inference on Water Content in the Mantle Transition Zone Near Subducted Slabs From Anisotropy Tomography, *Geochemistry, Geophysics, Geosystems*, *20*(2), 1189-1201, doi:10.1029/2018gc008090.

Conrad, C. P., T. A. Bianco, E. I. Smith, and P. Wessel (2011), Patterns of intraplate volcanism controlled by asthenospheric shear, *Nature Geoscience*, *4*(5), 317-321, doi:10.1038/ngeo1111.

Conrad, C. P., B. Steinberger, and T. H. Torsvik (2013), Stability of active mantle upwelling revealed by net characteristics of plate tectonics, *Nature*, *498*(7455), 479-482, doi:10.1038/nature12203.

Crowley, J. W., M. Gérault, and R. J. O'Connell (2011), On the relative influence of heat and water transport on planetary dynamics, *Earth and Planetary Science Letters*, *310*(3–4), 380-388, doi:10.1016/j.epsl.2011.08.035.

Demouchy, S., and N. Bolfan-Casanova (2016), Distribution and transport of hydrogen in the lithospheric mantle: A review, *Lithos*, *240-243*, 402-425, doi:https://doi.org/10.1016/j.lithos.2015.11.012.

Domeier, M., P. V. Doubrovine, T. H. Torsvik, W. Spakman, and A. L. Bull (2016), Global correlation of lower mantle structure and past subduction, *Geophysical Research Letters*, *43*(10), 4945-4953, doi:10.1002/2016GL068827.

Drewitt, J. W. E., M. J. Walter, J. P. Brodholt, J. M. R. Muir, and O. T. Lord (2022), Hydrous silicate melts and the deep mantle H_2O cycle, *Earth and Planetary Science Letters*, *581*, 117408, doi:https://doi.org/10.1016/j.epsl.2022.117408.

Fei, H., D. Yamazaki, M. Sakurai, N. Miyajima, H. Ohfuji, T. Katsura, and T. Yamamoto (2017), A nearly water-saturated mantle transition zone inferred from mineral viscosity, *Science Advances*, *3*(6), doi:10.1126/sciadv.1603024.

Goes, S., R. Agrusta, J. van Hunen, and F. Garel (2017), Subduction-transition zone interaction: A review, *Geopsphere*, *13*(7), 644-664, doi:10.1130/GES01476.1.

Goes, S., F. A. Capitanio, G. Morra, M. Seton, and D. Giardini (2011), Signatures of downgoing plate-buoyancy driven subduction in Cenozoic plate motions, *Physics of the Earth and Planetary Interiors*, *184*(1), 1-13, doi:https://doi.org/10.1016/j.pepi.2010.10.007.

Gomez, N., M. Yousefi, D. Pollard, R. M. DeConto, S. Sadai, A. Lloyd, A. Nyblade, D. A. Wiens, R. C. Aster, and T. Wilson (2024), The influence of realistic 3D mantle viscosity on Antarctica's contribution to future global sea levels, *Science Advances*, *10*(31), eadn1470, doi:doi:10.1126/sciadv.adn1470.

Hernlund, J. W., D. J. Stevenson, and P. J. Tackley (2008), Buoyant melting instabilities beneath extending lithosphere: 2. Linear analysis, *Journal of Geophysical Research: Solid Earth*, *113*(B4), doi:https://doi.org/10.1029/2006JB004863.

Hirschmann, M. M. (2006), Water, melting, and the deep earth H20 cycle, *Annual Review of Earth and Planetary Sciences*, *34*(1), 629-653, doi:10.1146/annurev.earth.34.031405.125211.

Houser, C. (2016), Global seismic data reveal little water in the mantle transition zone, *Earth and Planetary Science Letters*, *448*, 94-101, doi:http://dx.doi.org/10.1016/j.epsl.2016.04.018.

Huang, X., Y. Xu, and S.-i. Karato (2005), Water content in the transition zone from electrical conductivity of wadsleyite and ringwoodite, *Nature*, *434*(7034), 746-749, doi:10.1038/nature03426.

Kameyama, M., and R. Nishioka (2012), Generation of ascending flows in the Big Mantle Wedge (BMW) beneath northeast Asia induced by retreat and stagnation of subducted slab, *Geophysical Research Letters*, *39*(10), doi:https://doi.org/10.1029/2012GL051678.

Karato, S.-i. (2011), Water distribution across the mantle transition zone and its implications for global material circulation, *Earth and Planetary Science Letters*, *301*(3–4), 413-423, doi:10.1016/j.epsl.2010.11.038.
Karato, S.-i., B. Karki, and J. Park (2020), Deep mantle melting, global water circulation and its implications for the stability of the ocean mass, *Progress in Earth and Planetary Science*, *7*(1), 76, doi:10.1186/s40645-020-00379-3.
Karlsen, K. S., C. P. Conrad, M. Domeier, and R. G. Trønnes (2021), Spatiotemporal Variations in Surface Heat Loss Imply a Heterogeneous Mantle Cooling History, *Geophysical Research Letters*, *48*(6), e2020GL092119, doi:https://doi.org/10.1029/2020GL092119.
Karlsen, K. S., C. P. Conrad, and V. Magni (2019), Deep Water Cycling and Sea Level Change Since the Breakup of Pangea, *Geochemistry, Geophysics, Geosystems*, *20*(6), 2919-2935, doi:10.1029/2019GC008232.
Karlsen, K. S., M. Domeier, C. Gaina, and C. P. Conrad (2020), A tracer-based algorithm for automatic generation of seafloor age grids from plate tectonic reconstructions, *Computers & Geosciences*, *140*, 104508, doi:https://doi.org/10.1016/j.cageo.2020.104508.
Katz, R. F., M. Spiegelman, and C. H. Langmuir (2003), A new parameterization of hydrous mantle melting, *Geochemistry, Geophysics, Geosystems*, *4*(9), doi:https://doi.org/10.1029/2002GC000433.
Kelbert, A., A. Schultz, and G. Egbert (2009), Global electromagnetic induction constraints on transition-zone water content variations, *Nature*, *460*(7258), 1003-1006, doi:10.1038/nature08257.
King, S. D., and J. Ritsema (2000), African Hot Spot Volcanism: Small-Scale Convection in the Upper Mantle Beneath Cratons, *Science*, *290*(5494), 1137-1140, doi:10.1126/science.290.5494.1137.
Komabayashi, T., and S. Omori (2006), Internally consistent thermodynamic data set for dense hydrous magnesium silicates up to 35GPa, 1600°C: Implications for water circulation in the Earth's deep mantle, *Physics of the Earth and Planetary Interiors*, *156*(1), 89-107, doi:https://doi.org/10.1016/j.pepi.2006.02.002.
Kuritani, T., E. Ohtani, and J.-I. Kimura (2011), Intensive hydration of the mantle transition zone beneath China caused by ancient slab stagnation, *Nature Geosci*, *4*(10), 713-716, doi:http://dx.doi.org/10.1038/ngeo1250.
Kuritani, T., Q.-K. Xia, J.-I. Kimura, J. Liu, K. Shimizu, T. Ushikubo, D. Zhao, M. Nakagawa, and S. Yoshimura (2019), Buoyant hydrous mantle plume from the mantle transition zone, *Scientific Reports*, *9*(1), 6549, doi:10.1038/s41598-019-43103-y.
Lehnert, K., Y. Su, C. H. Langmuir, B. Sarbas, and U. Nohl (2000), A global geochemical database structure for rocks, *Geochemistry, Geophysics, Geosystems*, *1*(5), doi:https://doi.org/10.1029/1999GC000026.
Long, X., M. D. Ballmer, A. M.-C. Córdoba, and C.-F. Li (2019), Mantle Melting and Intraplate Volcanism Due to Self-Buoyant Hydrous Upwellings From the Stagnant Slab That Are Conveyed by Small-Scale Convection, *Geochemistry, Geophysics, Geosystems*, *20*(11), 4972-4997, doi:10.1029/2019gc008591.
Luth, R. W. (2003), 2.07 - Mantle Volatiles—Distribution and Consequences, in *Treatise on Geochemistry*, edited by H. D. Holland and K. K. Turekian, pp. 319-361, Pergamon, Oxford, doi:https://doi.org/10.1016/B0-08-043751-6/02124-1.
Magni, V., P. Bouilhol, and J. van Hunen (2014), Deep water recycling through time, *Geochemistry, Geophysics, Geosystems*, *15*(11), 4203-4216, doi:10.1002/2014GC005525.
Matthews, K. J., K. T. Maloney, S. Zahirovic, S. E. Williams, M. Seton, and R. D. Müller (2016), Global plate boundary evolution and kinematics since the late Paleozoic, *Global and Planetary Change*, *146*(Supplement C), 226-250, doi:10.1016/j.gloplacha.2016.10.002.
Meier, U., J. Trampert, and A. Curtis (2009), Global variations of temperature and water content in the mantle transition zone from higher mode surface waves, *Earth and Planetary Science Letters*, *282*(1), 91-101, doi:https://doi.org/10.1016/j.epsl.2009.03.004.

Motoki, M. H., and M. D. Ballmer (2015), Intraplate volcanism due to convective instability of stagnant slabs in the mantle transition zone, *Geochemistry, Geophysics, Geosystems*, *16*(2), 538-551, doi:https://doi.org/10.1002/2014GC005608.

Müller, R. D., J. Cannon, X. Qin, R. J. Watson, M. Gurnis, S. Williams, T. Pfaffelmoser, M. Seton, S. H. J. Russell, and S. Zahirovic (2018), GPlates: Building a Virtual Earth Through Deep Time, *Geochemistry, Geophysics, Geosystems*, *19*(7), 2243-2261, doi:doi:10.1029/2018GC007584.

Nestola, F., and J. R. Smyth (2016), Diamonds and water in the deep Earth: a new scenario, *International Geology Review*, *58*(3), 263-276, doi:10.1080/00206814.2015.1056758.

Ohtani, E., L. Yuan, I. Ohira, A. Shatskiy, and K. Litasov (2018), Fate of water transported into the deep mantle by slab subduction, *Journal of Asian Earth Sciences*, *167*, 2-10, doi:https://doi.org/10.1016/j.jseaes.2018.04.024.

Pearson, D. G., et al. (2014), Hydrous mantle transition zone indicated by ringwoodite included within diamond, *Nature*, *507*(7491), 221-224, doi:10.1038/nature13080.

Peslier, A. H., M. Schönbächler, H. Busemann, and S.-I. Karato (2017), Water in the Earth's Interior: Distribution and Origin, *Space Science Reviews*, *212*(1), 743-810, doi:10.1007/s11214-017-0387-z.

Ramirez, F. D. C., C. P. Conrad, and K. Selway (2023), Grain size reduction by plug flow in the wet oceanic upper mantle explains the asthenosphere's low seismic Q zone, *Earth and Planetary Science Letters*, *616*, 118232, doi:https://doi.org/10.1016/j.epsl.2023.118232.

Ramirez, F. D. C., K. Selway, C. P. Conrad, and C. Lithgow-Bertelloni (2022), Constraining Upper Mantle Viscosity Using Temperature and Water Content Inferred From Seismic and Magnetotelluric Data, *Journal of Geophysical Research: Solid Earth*, *127*(8), e2021JB023824, doi:https://doi.org/10.1029/2021JB023824.

Rüpke, L. H., J. P. Morgan, M. Hort, and J. A. D. Connolly (2004), Serpentine and the subduction zone water cycle, *Earth and Planetary Science Letters*, *223*(1–2), 17-34, doi:10.1016/j.epsl.2004.04.018.

Schmandt, B., S. D. Jacobsen, T. W. Becker, Z. Liu, and K. G. Dueker (2014), Dehydration melting at the top of the lower mantle, *Science*, *344*(6189), 1265-1268, doi:10.1126/science.1253358.

Schulze, K., H. Marquardt, T. Kawazoe, T. Boffa Ballaran, C. McCammon, M. Koch-Müller, A. Kurnosov, and K. Marquardt (2018), Seismically invisible water in Earth's transition zone?, *Earth and Planetary Science Letters*, *498*, 9-16, doi:https://doi.org/10.1016/j.epsl.2018.06.021.

Shephard, G. E., K. J. Matthews, K. Hosseini, and M. Domeier (2017), On the consistency of seismically imaged lower mantle slabs, *Scientific Reports*, *7*(1), 10976, doi:10.1038/s41598-017-11039-w.

Shirey, S. B., L. S. Wagner, M. J. Walter, D. G. Pearson, and P. E. van Keken (2021), Slab Transport of Fluids to Deep Focus Earthquake Depths—Thermal Modeling Constraints and Evidence From Diamonds, *AGU Advances*, *2*(2), e2020AV000304, doi:https://doi.org/10.1029/2020AV000304.

Suetsugu, D., T. Inoue, A. Yamada, D. Zhao, and M. Obayashi (2006), Towards Mapping the Three-Dimensional Distribution of Water in the Transition Zone from P-Velocity Tomography and 660-Km Discontinuity Depths, in *Earth's Deep Water Cycle*, edited, pp. 237-249, doi:https://doi.org/10.1029/168GM18.

Syracuse, E. M., P. E. van Keken, and G. A. Abers (2010), The global range of subduction zone thermal models, *Physics of the Earth and Planetary Interiors*, *183*(1–2), 73-90, doi:http://dx.doi.org/10.1016/j.pepi.2010.02.004.

Thompson, A. B. (1992), Water in the Earth's upper mantle, *Nature*, *358*(6384), 295-302, doi:10.1038/358295a0.

Torsvik, T. H., B. Steinberger, L. D. Ashwal, P. V. Doubrovine, and R. G. Trønnes (2016), Earth evolution and dynamics—a tribute to Kevin Burke, *Canadian Journal of Earth Sciences*, *53*(11), 1073-1087, doi:10.1139/cjes-2015-0228.

Torsvik, T. H., B. Steinberger, G. E. Shephard, P. V. Doubrovine, C. Gaina, M. Domeier, C. P. Conrad, and W. W. Sager (2019), Pacific-Panthalassic Reconstructions: Overview, Errata and the Way Forward, *Geochemistry, Geophysics, Geosystems*, *20*(7), 3659-3689, doi:10.1029/2019gc008402.

Valentine, G. A., and N. Hirano (2010), Mechanisms of low-flux intraplate volcanic fields—Basin and Range (North America) and northwest Pacific Ocean, *Geology*, *38*(1), 55-58, doi:10.1130/g30427.1.

van der Meer, D. G., D. J. J. van Hinsbergen, and W. Spakman (2018), Atlas of the underworld: Slab remnants in the mantle, their sinking history, and a new outlook on lower mantle viscosity, *Tectonophysics*, *723*, 309-448, doi:https://doi.org/10.1016/j.tecto.2017.10.004.

van Keken, P. E., B. R. Hacker, E. M. Syracuse, and G. A. Abers (2011), Subduction factory: 4. Depth-dependent flux of H2O from subducting slabs worldwide, *J. Geophys. Res.*, *116*(B1), B01401, doi:10.1029/2010jb007922.

Walter, M. J. (2021), Water transport to the core–mantle boundary, *National Science Review*, *8*(4), doi:10.1093/nsr/nwab007.

Wang, X.-C., S. A. Wilde, Q.-L. Li, and Y.-N. Yang (2015), Continental flood basalts derived from the hydrous mantle transition zone, *Nature Communications*, *6*(1), 7700, doi:10.1038/ncomms8700.

Wirth, R., C. Vollmer, F. Brenker, S. Matsyuk, and F. Kaminsky (2007), Inclusions of nanocrystalline hydrous aluminium silicate "Phase Egg" in superdeep diamonds from Juina (Mato Grosso State, Brazil), *Earth and Planetary Science Letters*, *259*(3), 384-399, doi:https://doi.org/10.1016/j.epsl.2007.04.041.

Wright, K. (2006), Atomistic Models of OH Defects in Nominally Anhydrous Minerals, *Reviews in Mineralogy and Geochemistry*, *62*(1), 67-83, doi:10.2138/rmg.2006.62.4.

Xing, K.-C., F. Wang, F.-Z. Teng, W.-L. Xu, Y.-N. Wang, D.-B. Yang, H.-L. Li, and Y.-C. Wang (2024), Potassium isotopic evidence for recycling of surface water into the mantle transition zone, *Nature Geoscience*, doi:10.1038/s41561-024-01452-y.

Yang, J., and M. Faccenda (2020), Intraplate volcanism originating from upwelling hydrous mantle transition zone, *Nature*, *579*(7797), 88-91, doi:10.1038/s41586-020-2045-y.

Young, A., N. Flament, K. Maloney, S. Williams, K. Matthews, S. Zahirovic, and R. D. Müller (2019), Global kinematics of tectonic plates and subduction zones since the late Paleozoic Era, *Geoscience Frontiers*, *10*(3), 989-1013, doi:https://doi.org/10.1016/j.gsf.2018.05.011.

Zhang, H., G. D. Egbert, and Q. Huang (2022), A relatively dry mantle transition zone revealed by geomagnetic diurnal variations, *Science Advances*, *8*(31), eabo3293, doi:doi:10.1126/sciadv.abo3293.

Geochemistry, Geophysics, Geosystems

Supporting Information for

Hydrous regions of the mantle transition zone lie beneath areas of intraplate volcanism

Helene Wang[1,2], Valentina Magni[1,3], Clinton P. Conrad[1,4,*] and Mathew Domeier[1,4]

[1] Centre for Earth Evolution and Dynamics (CEED), University of Oslo, Oslo, Norway

[2] TGS, Oslo, Norway

[3] Norwegian Geotechnical Institute (NGI), Oslo, Norway

[4] Centre for Planetary Habitability (PHAB), University of Oslo, Oslo, Norway

[*] Corresponding author: Clinton P. Conrad (c.p.conrad@geo.uio.no)

Contents of this file

Text S1 to S3
Figures S1 to S5

Text S1. Computing the regassing flux from the tectonic plate reconstruction

We follow the approach of *Karlsen et al.* [2019] to compute regassing rates from the tectonic reconstruction of *Matthews et al.* [2016], which has been corrected as described by *Torsvik et al.* [2019]. For each plate boundary segment that is identified as a subduction zone, we compute the mass of slab material subducted per unit time:

$$\frac{dM_l}{dt} = \rho v_s d L_s \qquad \text{(S1)}$$

where ρ, v_s, d, and L_s are the density, convergence velocity, thickness, and length of the subduction zone segment, respectively. We use a plate density of ρ=3200 kg/m^3. To find the regassing rate of the segment, we multiply equation S1 by nondimensional regassing factor α (described below), which describes the mass of subducting water as a fraction of the mass of the slab. Because most of this water is degassed through a volcanic arc, we also multiply by a fraction ε (described below), which *Karlsen et al.* [2019] defined as the fraction of the subducted water that descends into the deep mantle. The regassing water flux (R) is thus:

$$R = \alpha \varepsilon \rho v_s d L_s \qquad \text{(S2)}$$

The thickness *d* of the subducting slab depends on the age τ of the oceanic lithosphere:

$$d(\tau) = 2.32\sqrt{\kappa\tau} \qquad \text{(S3)}$$

where 80 Myr > τ > 10 Myr and $\kappa = 7.6 \cdot 10^{-7}$ m^2/s is the thermal diffusivity. For τ >80 Myr and τ<10 Myr, upper and lower bounds on plate thickness are set to 100 km and 36 km, respectively [*Sclater et al.*, 1980]. We applied a minimum velocity limit of 0.2 cm/yr to exclude inactive plate boundaries. This filtering mainly affects the total length of subduction zones, and does not significantly affect the total area of subducted seafloor [*Karlsen et al.*, 2019] because only inactive or very slowly converging trenches are removed. While both continental and oceanic subduction zones are included, any convergent boundaries that are not explicitly identified as a subduction zone in the tectonic reconstruction model (e.g., continental convergence) are ignored.

The nondimensional regassing factor α relates to the slab's initial bulk water content, and is a poorly constrained parameter [*Karlsen et al.*, 2019]. We chose a value of α that yields a present-day global H_2O subduction flux of $3.44 \cdot 10^{11}$ kg/yr to depths >230 km, which is within the range estimated by *van Keken et al.* [2011] and describes the "regassing-dominated" case of *Karlsen et al.* [2019]. Other studies have estimated both smaller [*Bodnar et al.*, 2013; *Faccenda et al.*, 2012; *Parai and Mukhopadhyay*, 2012; *Rüpke et al.*, 2004] or larger [*Hacker*, 2008; *Magni et al.*, 2014] regassing fluxes for the present Earth. We note that the choice of regassing factor mostly affects the magnitude of water content within the transition zone, and not the lateral variations of the heterogeneous distribution of water in the mantle.

The water retention factor ε expresses the fraction of the initial water content of the slab that reaches the deep mantle (below 410 km depth). Because colder and faster slabs remain colder at depth, and therefore can retain more water [*Magni et al.*, 2014; *van Keken et al.*, 2011], this factor depends on the thermal parameter $\Phi = v_s\tau$ of each specific subduction zone segment. *Karlsen et al.* [2019] expressed the water retention factor as $\varepsilon(\Phi) = max\left(0, a + b(1 - e^{-c\Phi})\right)$, and determined the constants *a*, *b* and *c* by fitting the function $\varepsilon(\Phi)$ to an independent study of slab water retention [*Rüpke et al.*, 2004]. Here we use $a = -0.1$, $b = 0.5$, and $c = 0.0023$, as given by *Karlsen et al.* [2019].

We computed ε for all individual subduction zone segments, for all times $t \in [0,400]$, and found that global mean values of ε vary between about 0.1 and 0.25. The mean value is about 0.14 for the present day (Fig. S1c). These values result in large variations in regassing rates, which range from about $0.35 \cdot 10^{12}$ kg/yr for the present day to more than $1.5 \cdot 10^{12}$ kg/yr at 125 Ma (Fig. S1e). Regional variations in the rate of water input into the mantle are significant, with older and faster slabs bringing water downward more rapidly (Fig. 2, left column).

Text S2. Distributing regassed water onto MTZ grid points

Regassed water from subduction is distributed within the MTZ onto global mesh of grid points (Figure S2, left). Each mesh point represents approximately 50000 km^2 on the Earth's surface (~225 km spacing), or ~40000 km^2 at the base of the MTZ. We distributed water from the segment among the *N* nearest neighbor points around the segment midpoint (Figure S2, right). The amount of water added to each k^{th} nearest neighbor mesh point is weighted by the distance from the segment midpoint. If d_k is the distance to the k^{th} nearest neighbor mesh point, then that point receives a fraction of water given by $\frac{D}{d_k}$ where $D = 1/\left(\sum_{i=1}^{N} \frac{1}{d_i}\right)$. Then the total water assigned to this point is:

$$M_k = \frac{R}{A} \Delta t \frac{\mathrm{D}}{d_k} \qquad \text{(S4)}$$

where M_k, R, A, and Δt are the water mass per area assigned to mesh point k, the regassing flux of the subduction segment (equation S2), the mesh point surface area, and the time step (i.e., 1 Myr). We found in tests that increasing *N* from 10 to 30, which increases the lateral spread of water from 390 km to 690 km, increases the fraction of "wet" grid points (defined using a threshold of $0.5 \cdot 10^9$ kg/km^2, see section 2.3) by less than 20% (Figure 7 of *Wang* [2022]). Thus, the effect of the choice of *N* is modest, and we use *N*=10 in this study. We note that the lateral spread of the water in the MTZ is more closely related to slab stagnation (Figure 5a). We thus account for slab stagnation by applying an MTZ residence time t_{MTZ}, and using a constant value of *N*=10 to distribute water within ~390 km of each subduction zone midpoint (Figure S2).

Text S3. Developing the intraplate volcanism (IPV) database

Using the criteria described in the main text, we extracted 2096 IPV locations (Figure S3a) from the GEOROC (https://georoc.eu/) database [*Lehnert et al.*, 2000], after removing all duplicate points. Each location has a specified age range during which IPV was active. For example, 468 locations indicate currently active IPV samples with an age of 0 Ma (Figure S3b). For earlier times, we reconstructed the eruption locations of active IPV by applying the GPlates [*Müller et al.*, 2018] continent polygon files from the tectonic reconstruction of *Matthews et al.* [2016], corrected as described by *Torsvik et al.* [2019]. By assigning each previously-active IPV point to a continental polygon, itself associated with a representative plate (i.e., its PlateID), the IPV points are rotated, along with their continental polygons, back to their locations at the time of eruption. Typically, samples are defined using an age range, instead of a specific eruption time. We reconstruct these IPV points backward onto maps for each 1 Myr age increment within the point's given age range. For a few points, this age range was limited by the age range of the continental polygon associated with the IPV point.

We note that many IPV observations are positioned in the near vicinity of each other (with a spacing closer than our grid spacing of ~225 km), and are likely associated with the same volcanic eruption. Thus, where several IPV points are associated with the same mesh point on a given age map, we merged the cluster into one single point with the coordinates of the mesh point (Figure S3b). The above exclusions narrow the number of present-day active intraplate volcanic samples to 132 (Figure 2l). This filtering has been applied to each timestep in the considered time range (Figure 2, right column), resulting in a changing number of IPV points for each timestep (Figure S3c). Because many samples are defined using an age range, we find extended periods with a relatively constant number of IPV samples, broken by jumps in the number of samples. The number of IPV data points is smaller in the past because the geologic record of IPV becomes increasingly erased backward in time.

Text S4. Constructing random rotations of the MTZ hydration maps

We generated random rotations following the approach of *Miles* [1965], who showed that a uniform distribution of rotation poles on the Earth's surface, coupled with rotation angles drawn from the distribution $(\theta - sin\theta)/\pi$ (where $0 \leq \theta \leq \pi$), produces a uniform distribution of random re-orientations. Thus, an object on Earth's surface (e.g., an MTZ hydration map) can be randomly-reoriented to a new position on Earth's surface using this procedure. We show a few examples of randomly re-oriented MTZ hydration maps, and their correlations with (unrotated) IPV, in Figure S5.

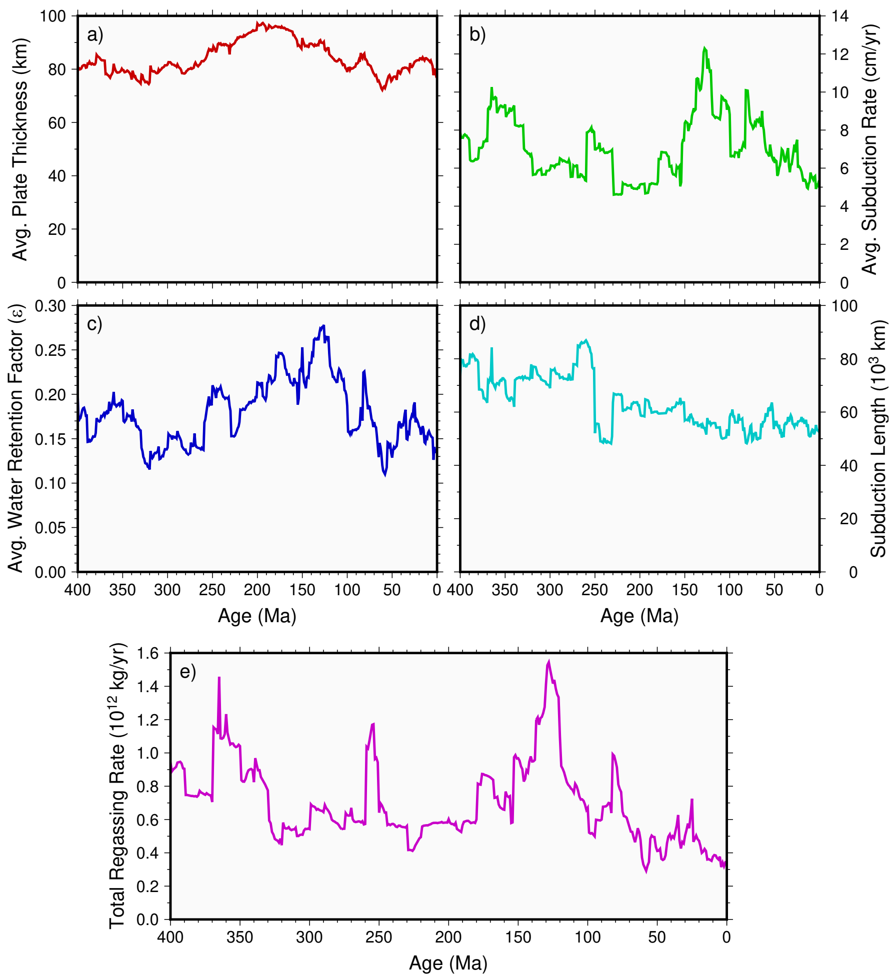

Figure S1. Parameters used to compute rates of regassing into the deep mantle, showing (a) the global average plate thickness, (b) the global average subduction rate, (c) the global average water retention fraction ε, and (d) the total length of global subduction zones. These parameters are combined using equation S2, as described in Supplementary Text S1 to compute the regassing rate $\boldsymbol{R}$ [kg/m/year] along each subduction zone segment (Figure 2, left column). The summed regassing along all segments gives the (e) global total regassing flux, which varies significantly a function of time since 400 Ma.

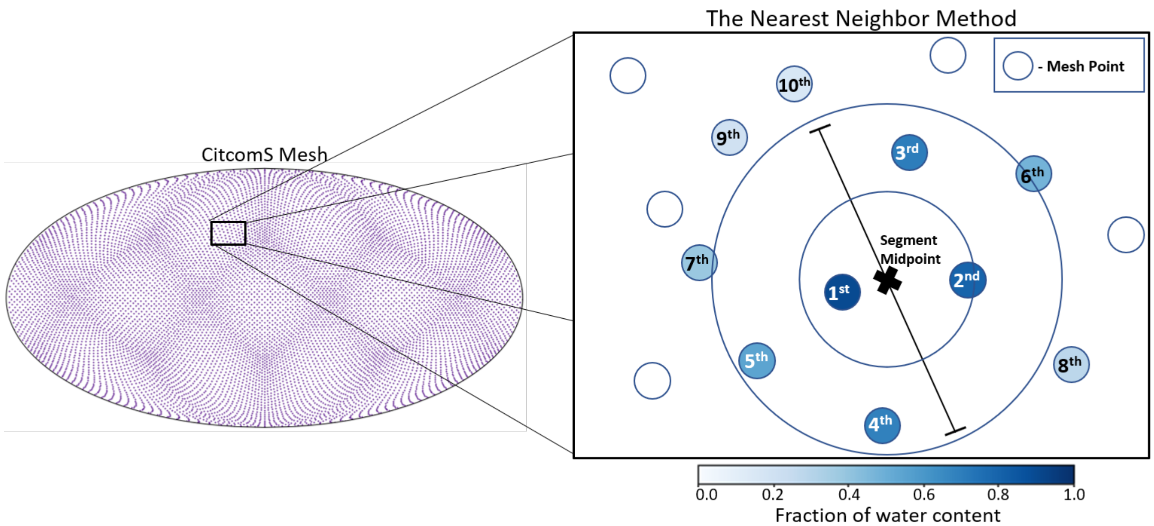

Figure S2. Assignment of water from a subduction zone segment to mesh grid points. The left-hand figure shows the global mesh point locations (purple, 10094 global mesh points positioned based on the CitcomS spherical finite element code [*Zhong et al.*, 2000]) using a Mollweide projection. In this grid, 12 diamond-shaped "caps" facilitate a relatively uniform distance between the mesh points on a spherical surface. On the right, an illustration of the nearest neighbor method shows a segment and its midpoint (marked with an X) and the *N* nearest neighbor mesh points (here, *N*=10). These points each receive a weighted relative fraction of the total water content (blue color, see equation S4) that is "regassed" to Earth's mantle at this segment midpoint. Grid points closer to the segment midpoint receive more water (darker blue), while more distant points receive less (lighter blue). Mesh points that are not among the *N*=10 closest points to the segment midpoint do not receive any water (white).

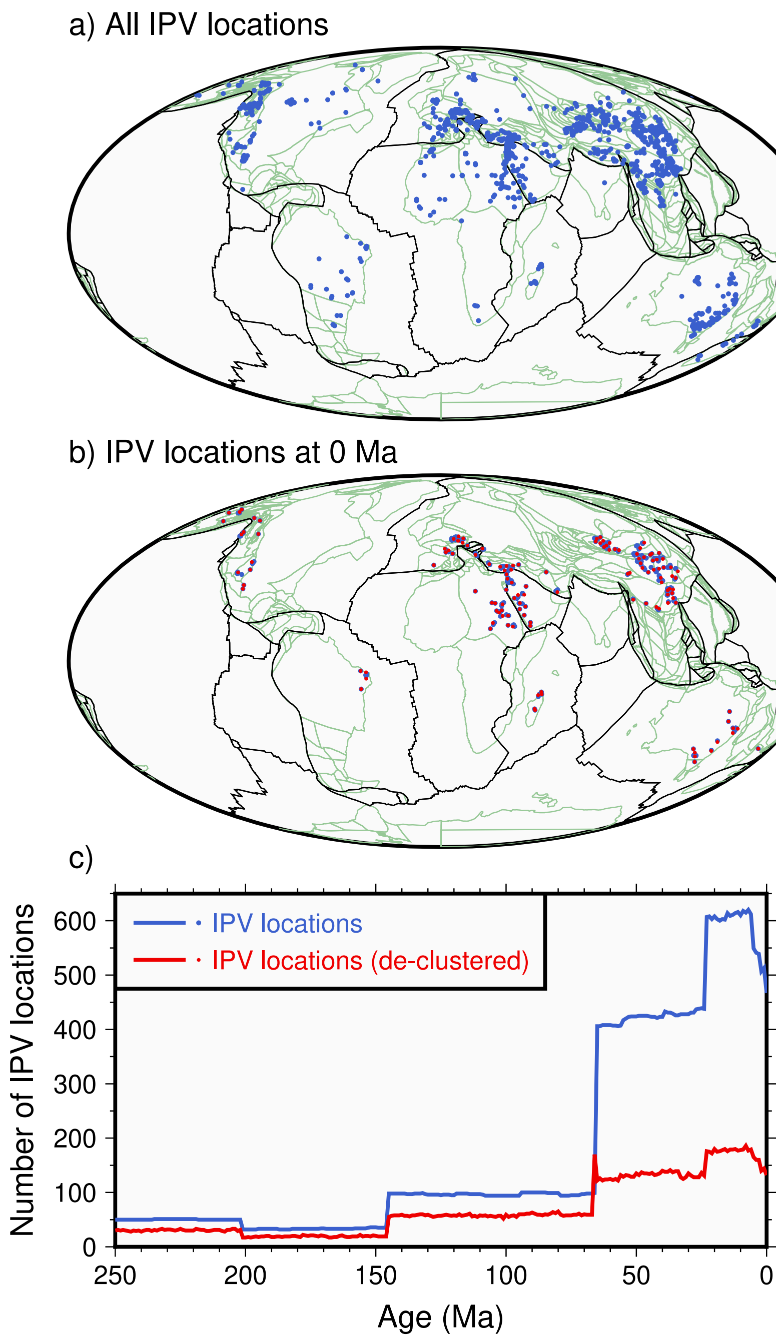

Figure S3. Intraplate volcanism (IPV) samples extracted from the GEOROC (https://georoc.eu/) database [*Lehnert et al.*, 2000]. Shown in (a) are the 2095 IPV locations with eruption ages between 0 and 250 Ma (blue dots). Shown in (b) are the 467 IPV locations with 0 Ma age (blue dots), which define 132 IPV locations after de-clustering (red dots, see Supplementary Text S3). Shown in (c) are the number of different IPV locations as a function of age between 250 and 0 Ma, for both all IPV locations (blue line) and for the de-clustered locations (red line).

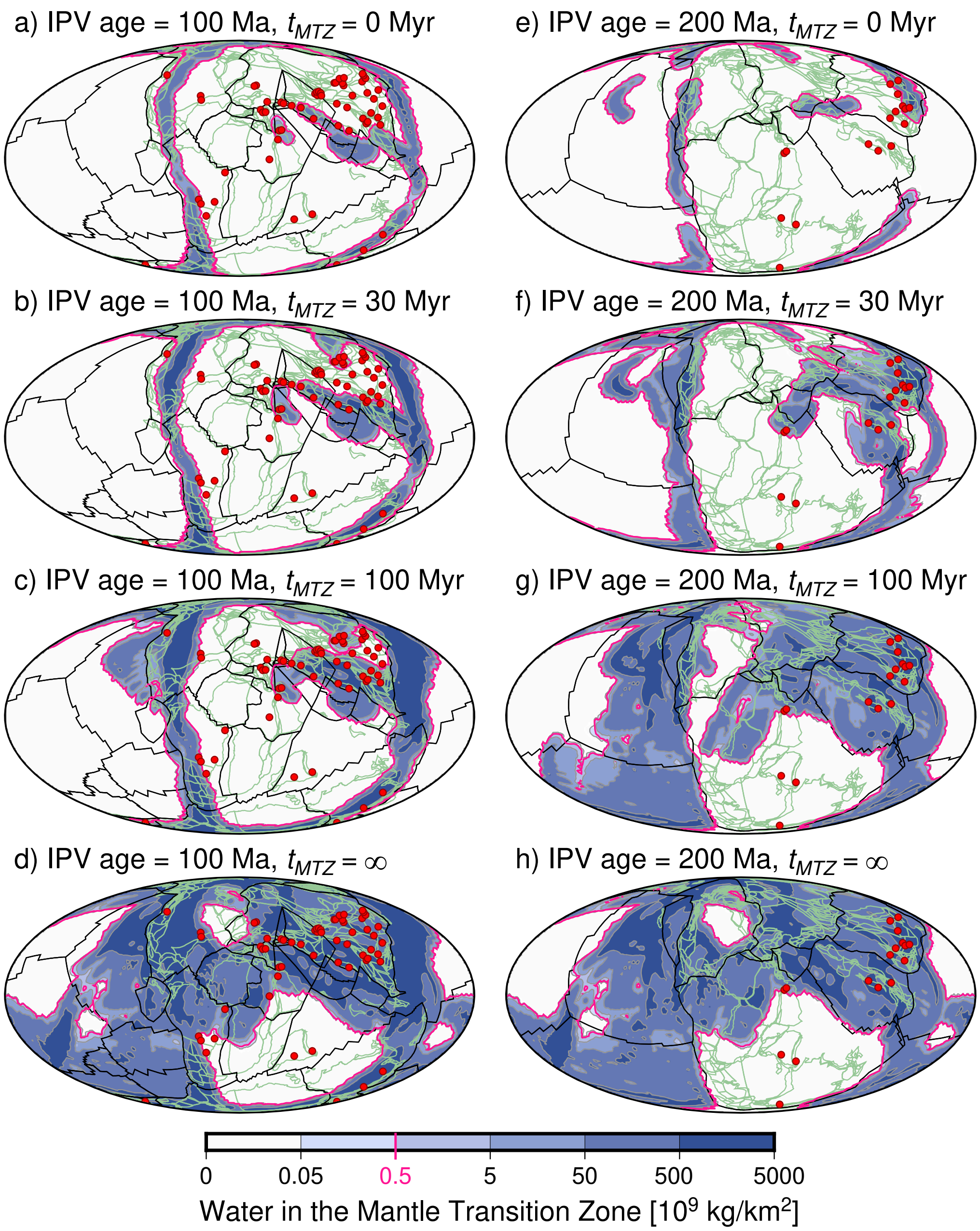

Figure S4. Effect of varying MTZ water residence time, shown at 100 Ma (left column, a-d) and 200 Ma (right column, e-h). Predictions of the water distribution in the mantle transition zone (MTZ) are shown using colors (as for Figure 3), with locations of active intraplate volcanism (IPV) shown by red dots. The slab sinking rate is v_{sink} = 3 cm/yr, and there is a t_{IPV} = 20 Myr IPV delay. The MTZ water residence time is (a, e) t_{MTZ} = 0 Myr, (b, f) t_{MTZ} = 30 Myr, (c, g) t_{MTZ} = 100 Myr, and (d, h) $t_{MTZ} = \infty$, meaning that water that reaches the MTZ stays there.

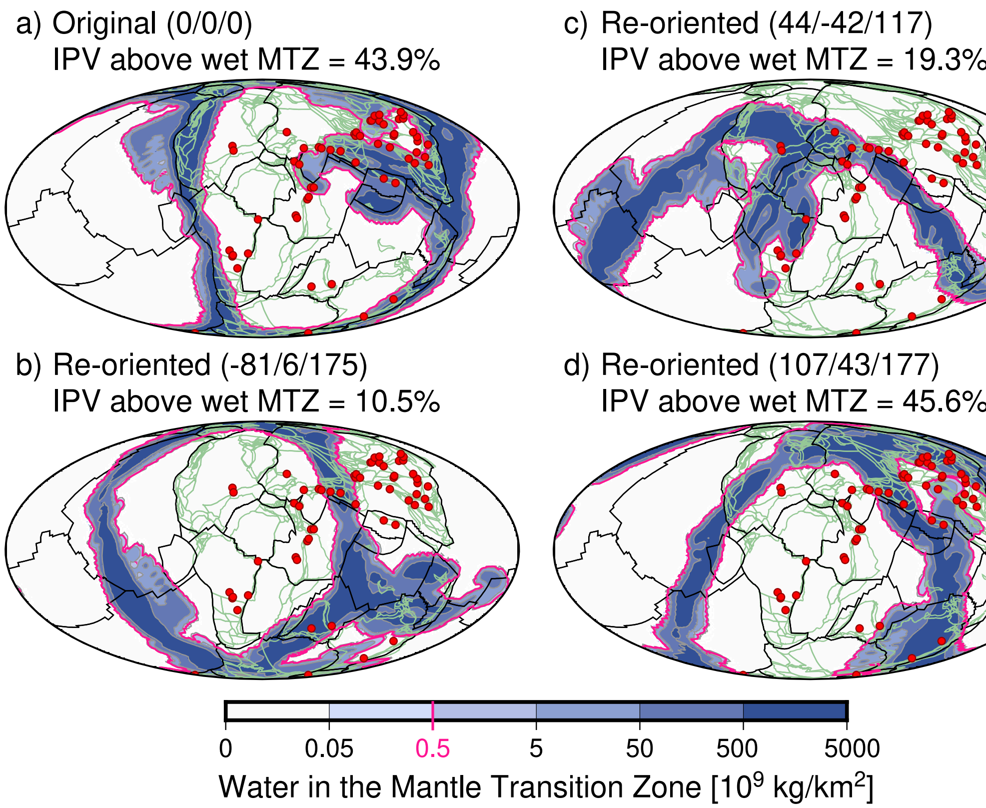

Figure S5. Examples showing the re-orientation of the MTZ water grid. The illustration displays the mantle transition zone (MTZ) water grid at 125 Ma with an MTZ water residence time of t_{MTZ} = 100 Myr, a slab sinking rate of v_{sink}=3 cm/yr, and IPV delay period of t_{IPV} = 20 Myr, i.e., the reference scenario of this study. Four re-orientations of this grid, defined by random choices of longitude/latitude/rotation (above each figure, in degrees) are shown. Stationary intraplate volcanism (IPV) locations (red dots), reconstructed coastlines (green lines), and plate boundaries (black lines) are also displayed (these are not rotated with the MTZ water grid). The percentage of IPV samples above wet MTZ values (i.e., ≥ 0.5 $\cdot 10^9$ kg/km^2, pink contour) are given for each water grid rotation.

References

Bodnar, R. J., T. Azbej, S. P. Becker, C. Cannatelli, A. Fall, and M. J. Severs (2013), Whole Earth geohydrologic cycle, from the clouds to the core: The distribution of water in the dynamic Earth system, *Geological Society of America Special Papers*, *500*, 431-461, doi:10.1130/2013.2500(13).

Faccenda, M., T. V. Gerya, N. S. Mancktelow, and L. Moresi (2012), Fluid flow during slab unbending and dehydration: Implications for intermediate-depth seismicity, slab weakening and deep water recycling, *Geochem. Geophys. Geosyst.*, *13*, Q01010, doi:10.1029/2011gc003860.

Hacker, B. R. (2008), H2O subduction beyond arcs, *Geochem. Geophys. Geosyst.*, *9*(3), Q03001, doi:10.1029/2007gc001707.

Karlsen, K. S., C. P. Conrad, and V. Magni (2019), Deep Water Cycling and Sea Level Change Since the Breakup of Pangea, *Geochemistry, Geophysics, Geosystems*, *20*(6), 2919-2935, doi:10.1029/2019GC008232.

Lehnert, K., Y. Su, C. H. Langmuir, B. Sarbas, and U. Nohl (2000), A global geochemical database structure for rocks, *Geochemistry, Geophysics, Geosystems*, *1*(5), doi:https://doi.org/10.1029/1999GC000026.

Magni, V., P. Bouilhol, and J. van Hunen (2014), Deep water recycling through time, *Geochemistry, Geophysics, Geosystems*, *15*(11), 4203-4216, doi:10.1002/2014GC005525.

Matthews, K. J., K. T. Maloney, S. Zahirovic, S. E. Williams, M. Seton, and R. D. Müller (2016), Global plate boundary evolution and kinematics since the late Paleozoic, *Global and Planetary Change*, *146*(Supplement C), 226-250, doi:10.1016/j.gloplacha.2016.10.002.

Miles, R. E. (1965), On Random Rotations in R^3, *Biometrika*, *52*(3/4), 636-639, doi:10.2307/2333716.

Müller, R. D., J. Cannon, X. Qin, R. J. Watson, M. Gurnis, S. Williams, T. Pfaffelmoser, M. Seton, S. H. J. Russell, and S. Zahirovic (2018), GPlates: Building a Virtual Earth Through Deep Time, *Geochemistry, Geophysics, Geosystems*, *19*(7), 2243-2261, doi:doi:10.1029/2018GC007584.

Parai, R., and S. Mukhopadhyay (2012), How large is the subducted water flux? New constraints on mantle regassing rates, *Earth and Planetary Science Letters*, *317–318*(0), 396-406, doi:10.1016/j.epsl.2011.11.024.

Rüpke, L. H., J. P. Morgan, M. Hort, and J. A. D. Connolly (2004), Serpentine and the subduction zone water cycle, *Earth and Planetary Science Letters*, *223*(1–2), 17-34, doi:10.1016/j.epsl.2004.04.018.

Sclater, J. G., C. Jaupart, and D. Galson (1980), The heat flow through oceanic and continental crust and the heat loss of the Earth, *Reviews of Geophysics*, *18*(1), 269-311, doi:https://doi.org/10.1029/RG018i001p00269.

Torsvik, T. H., B. Steinberger, G. E. Shephard, P. V. Doubrovine, C. Gaina, M. Domeier, C. P. Conrad, and W. W. Sager (2019), Pacific-Panthalassic Reconstructions: Overview, Errata and the Way Forward, *Geochemistry, Geophysics, Geosystems*, *20*(7), 3659-3689, doi:10.1029/2019gc008402.

van Keken, P. E., B. R. Hacker, E. M. Syracuse, and G. A. Abers (2011), Subduction factory: 4. Depth-dependent flux of H2O from subducting slabs worldwide, *J. Geophys. Res.*, *116*(B1), B01401, doi:10.1029/2010jb007922.

Wang, H. (2022), Hydrous Regions of the Mantle Transition Zone Affect Patterns of Intraplate Volcanism, University of Oslo.

Zhong, S. J., M. T. Zuber, L. Moresi, and M. Gurnis (2000), Role of temperature-dependent viscosity and surface plates in spherical shell models of mantle convection, *Journal of Geophysical Research-Solid Earth*, *105*(B5), 11063-11082, doi:10.1029/2000jb900003.